General Disclaimer

One or more of the Following Statements may affect this Document

- This document has been reproduced from the best copy furnished by the organizational source. It is being released in the interest of making available as much information as possible.

- This document may contain data, which exceeds the sheet parameters. It was furnished in this condition by the organizational source and is the best copy available.

- This document may contain tone-on-tone or color graphs, charts and/or pictures, which have been reproduced in black and white.

- This document is paginated as submitted by the original source.

- Portions of this document are not fully legible due to the historical nature of some of the material. However, it is the best reproduction available from the original submission.

4-302

NBS REPORT
9774

SPECTRAL REFLECTIVITY OF SOLID SURFACES AT LOW TEMPERATURES

M. C. Jones and D. C. Palmer

U. S. DEPARTMENT OF COMMERCE
NATIONAL BUREAU OF STANDARDS
Institute for Basic Standards
Boulder, Colorado 80302

NATIONAL BUREAU OF STANDARDS REPORT

NBS PROJECT		NBS REPORT
2750474	October 26, 1970	9774

SPECTRAL REFLECTIVITY OF SOLID SURFACES AT LOW TEMPERATURES

Report to

National Aeronautics and Space Administration
NASA Technical Supervisor: Dr. Klaus Schocken
George C. Marshall Space Flight Center
Huntsville, Alabama
Prepared under Government Orders H2153A and H62437A

by

M. C. Jones and D. C. Palmer

Cryogenics Division
Institute for Basic Standards
National Bureau of Standards
Boulder, Colorado

U.S. DEPARTMENT OF COMMERCE
NATIONAL BUREAU OF STANDARDS

TABLE OF CONTENTS

Table of Contents (Continued)

LIST OF FIGURES AND TABLES

List of Figures and Tables (Continued)

SPECTRAL REFLECTIVITY OF SOLID SURFACES AT LOW TEMPERATURES

by

M. C. Jones and D. C. Palmer

ABSTRACT

In Part I experimental data are presented for the normal spectral absorptivity of the transition metals nickel, iron, platinum and chromium at both room and liquid helium temperatures in the wavelength range 2.5 to 50 μm. The absorptivity was derived from reflectivity measurements made relative to a room-temperature vapor-deposited gold reference mirror. The absorptivity of the gold reference mirror was measured calorimetrically using infrared laser sources. Investigation of various methods of sample surface preparation resulted in the choice of a vacuum annealing process as the final stage.

Results are compared to calculations based on a 2-band model. The first band is identified with the s-electrons but it is necessary to determine material parameters for the second band empirically. The temperature and wavelength dependence of the absorptivities of nickel and iron can be represented only qualitatively, but for platinum quite well if second band parameters are assumed to be temperature independent. The Anomalous Skin Effect theory gives a better account of the temperature dependence than the classical or local theory and in all

cases agreement is improved if the relaxation time for the s-electrons is calculated according to the theory of the quantum mechanical interaction due to Holstein and Gurzhi. In the case of chromium no comparison with the theory is made since an absorptivity maximum at about 10 μm appears in the low temperature results. This feature has been identified previously by others as due to the onset of antiferromagnetism. The absorptivity in the region of the maximum is the same at 7.5 K as at 76.5 K.

In Part II the same technique is used to measure the normal spectral reflectivity of an indium antimonide sample at 10.5 K. The data are fitted to a classical reflectivity function from which an accurate value for the reststrahlen frequency is obtained. A discussion is given of a theory of the reststrahlen frequency under development.

PART I. THE INFRARED ABSORPTIVITY OF TRANSITION METALS AT ROOM AND LOW TEMPERATURES

1. Introduction

Knowledge of the infrared optical properties of metals at low temperatures is important in the thermal balancing of spacecraft and in a variety of cryogenic insulation problems both of the conventional type and those involving multiple layers of polished metal alternating with a dielectric ("multilayer" insulation). A previous survey[1] showed that little data existed in the literature. Furthermore, the available data were usually at short wavelengths ($\leq 10\ \mu$ m), were often in the form of optical constants and were rarely available for the more common structural metals which are usually transition metals and their alloys. In addition, data at room temperature were often not available for a sample whose low temperature properties were given. In contrast many studies of a variety of metals at room temperature have been available in the literature for a number of years, although, here too, long wavelengths have been neglected owing to instrumentation difficulties. The present paper is an outcome of the above noted survey. In it an attempt is made to rectify some of these shortcomings by reporting a study of the transition metals--iron, nickel, platinum, and chromium--at room temperature and at about 9 K. The wavelength range is from $2.5\ \mu$ m to $50\ \mu$ m.

In the experiments to be described the property measured was the normal, spectral reflectivity of a sample at room or liquid helium temperature relative to that of a known reference sample (see figures 1 and 2). The latter was a high quality vapor deposited gold film, which was maintained at room temperature at all times. In order to obtain the absorptivity, which is the property of most interest in application, the data were first converted to absolute reflectivities; then, by definition the normal absorptivity for a perfectly specular surface is (1.0 - normal absolute reflectivity).

The infrared absorptivity of metals is usually interpreted in terms of the interaction of an electromagnetic wave with the free electrons of the metal. The well known Drudé single electron theory[2] has been applied with varying degrees of success to noble and alkali metals at room and higher temperatures. Except at very short wavelengths (say, less than 4 μm) the correct wavelength and temperature dependence is obtained if the relaxation time introduced in the theory is the d.c. relaxation time obtained from electrical conductivity measurements. However, in all but a few exceptional cases the relaxation time which fits the data is somewhat less than the literature value for the pure metal.

For pure metals at low temperatures it is also well established that the Drude theory must be modified to account for the long free paths

of the electrons if the correct wavelength and temperature dependence is to be obtained. The resulting Anomalous Skin Effect theory[3, 4] is mathematically formidable but computations are readily made on a computer. The correctness of this approach has been well verified for monovalent metals.[5, 6, 7] It is also well established[8, 9] that a second low temperature effect occurs, namely, the relaxation time becomes frequency dependent due to a quantum mechanical interaction between photon, phonon, and electron and the relaxation time can only be related to the d. c. relaxation time at frequencies below that corresponding to the Debye temperature[10, 11] (i. e. $\omega_o \equiv \frac{k\theta}{\hbar}$ where θ is the Debye temperature, $\hbar$ = Planck's constant divided by 2π and k = Boltzmann's constant). Above this frequency the excess of absorptivity over that which would be calculated from the d. c. relaxation time may be referred to as quantum absorption.

The transition metals, transition metal alloys, and some other polyvalent metals are not adequately treated by the Drude Single Electron theory. However, a very satisfactory description of their optical properties at room and high temperatures is based on a generalization of the single electron theory, the two band model, applied to optical properties by Roberts.[12, 13] The theory is in effect the same generalization as has been used for the interpretation of other transition metal properties, namely, the Hall effect, magnetoresistance, and

thermoelectric power and, as pointed out by Wilson,[14] is the simplest approximation which takes into account the anisotropy of the Fermi surface. This latter is assumed spherical in the Drude theory and the Anomalous Skin Effect theory. The theory amounts to introducing a second conduction band with different effective mass and relaxation time. The distinguishing feature of the transition metals is that they do not show a plateau in their absorptivity as a function of wavelength in the near infrared, a property clearly exhibited by monovalent metals and predicted by the Drude theory.

The Roberts theory has been very useful in predicting and correlating the absorptivities or emissivities of transition metals as a function of both temperature and wavelength at room and high temperatures. Two approaches have been used. In the first[15] the high temperature absorptivity has been predicted with moderate success from the Roberts theory using parameters applicable at room temperature, but requiring always that the equations should give the correct experimental d. c. conductivity in the limit of zero frequency. The second approach[16] recognizes that the layer of material at the surface in which the interaction with the electromagnetic wave occurs may not be characteristic of the pure annealed bulk material through surface work hardening. Therefore no attempt is made to associate parameters with known physical properties of the bulk material. Instead all

parameters are determined by the absorptivity data alone insofar as is possible: not all parameters are uniquely determined by the absorptivity data over a limited wavelength range. The latter approach is therefore an engineering correlation and lends itself well to the description in terms of absorptivity of commercial surfaces, impure metals, or surfaces which have received no special treatment to remove the work hardened layer. It has the disadvantage that the parameters obtained have somewhat obscure physical significance.

The purpose of the present study was to investigate the absorptivity of transition metals at room and low temperatures to determine whether a systematic procedure could be found for their prediction, which would be at the same time firmly based on physical principles. To this end it was decided to apply the first approach given above to room and low temperatures and to confine experiments to pure annealed metals with high quality surfaces representative in properties of the bulk material. If this should lead to a fruitful result the extension to less well characterized surfaces could easily be made using the second approach.

2. Preparation of Samples

In preparing a metal surface for optical or infrared property measurements there are two basic approaches for obtaining a surface representative of pure annealed bulk material. The first is by vapor deposition of a thick film on a flat glass or quartz substrate. The

second is by appropriate treatment of the mechanically polished surface of a piece of pure metal. While it has been demonstrated that at room temperature the former approach gives rise to some of the highest reflectivities yet observed for noble metals, [17] and this in turn has been attributed to the absence of lattice distortions normally caused by mechanical polishing, there are, nevertheless, some objections to the use of vapor deposited films. Firstly, at room temperature measured conductivities and densities differ significantly from those for pure bulk material even for high quality ultra-high-vacuum films. Secondly, for a thick opaque film which is still thin enough to conform to the smoothness of the substrate (typically ~2000 Å), the mean free path of the electron at liquid helium temperatures may greatly exceed the film thickness. In this case the effective relaxation time of the electrons is a function of the film thickness and will thus modify the observed reflectivity or absorptivity. Such observations would be extremely difficult to interpret. Hence in this work the second approach has been taken and efforts directed toward eliminating work-hardening at the surface.

The samples were prepared from highly purified, polycrystalline discs about 25 mm in diameter and 2-3 mm thickness. The manufacturer's stated purities were as follows: nickel 0.99997, iron 0.9999, platinum 0.99992 and chromium 0.99996. On reception the samples were first annealed for 30 minutes under a vacuum of 10^{-5} to 10^{-6} torr

at 1422 K. An evaluation of various methods of polishing was then carried out on nickel in order to select the best technique which was then to be applied to all samples. The criterion was the room-temperature near-infrared reflectivity since ample evidence exists[18, 19] to the effect that the reflectivity increases significantly when the work-hardened layer caused by mechanical polishing is removed. On the other hand it is also important to maintain flatness and smoothness especially in our measurements where the sample forms a mirror in the imaging system of the spectrophotometer. Previous work[19] indicated that for the apparatus used here, using the method of Newton's rings, the sample should be flat to within 5 fringes over a diameter of 1 cm. The flatness achieved here has been of the order of 1 fringe over a 1 cm diameter. As for smoothness the r.m.s. peak to valley roughness should be a good deal less than the wavelength of the incident radiation. No difficulty has been encountered using techniques described below in obtaining maximum peak to valley readings of 0.05μm using a stylus profilometer over distances of the order of a few mm.

The techniques applied to the nickel sample were as follows:

i) Mechanical polishing to high mirror finish followed by electropolishing at high current density (0.5 A/cm^2 in a 57% vol. solution of sulfuric acid and distilled water--time 30 sec.)

ii) Mechanical polishing to high mirror finish followed by electropolishing at low current density (0.03 to 0.1 A/cm^2; electrolyte as in i) with use of polishing wheel. In this case the electrolyte was continuously dripped onto a polishing cloth mounted on a brass metallographic polishing wheel rotating at 160 r.p.m. The polishing wheel was made the cathode and the sample the anode.

iii) Mechanical polishing followed by vacuum annealing at temperatures and times which according to the literature should give complete recrystallization (673 K for 1 hr.[21] For iron, platinum, and chromium appropriate recrystallization data is also available.[20, 22, 23]

Mechanical polishing was with successively finer grades of diamond and alumina abrasives and was always done by hand either on a cast iron lapping block or on polishing paper. Preparation was completed by washing with detergent solution and rinsing with distilled water.

Technique i) was rejected without further testing because even after several variations in procedure and cathode geometry the surface lost its specularity. This is an essential surface property for alignment of the reflectivity apparatus described below apart from considerations of surface smoothness referred to above. Technique ii) was applied for times and current densities which would have removed several μm

of surface material. The resulting surface was sufficiently specular but slightly irregularly polished to the eye; the degree of polishing appeared to depend on orientation of crystallites at the sample surface. Technique iii) produced a good specular surface. It is important in using this technique to keep the temperature as close to the 1 hr. recrystallization temperature as possible; it was observed that vacuum annealing at about 1000 K gave rise to thermal etching at the grain boundaries.

The room-temperature near-infrared reflectivities by techniques ii) and iii) are compared in figure 1 on the basis of which iii) was chosen for all other samples. It is noteworthy that Biondi[31] compared techniques i) and iii) and found very little difference in the absorptivity at liquid helium temperature. However, his samples were vacuum annealed at 1023 K to 1123 K for 12 hrs. which by our experience would have produced excessive thermal etching.

In preparing samples it was found that even higher reflectivity could sometimes be achieved by repeating the last stage of mechanical polishing and the vacuum annealing procedure. This improvement is also illustrated in figure 1 for nickel. In figure 1 and in figure 2 for platinum it is quite clear that the ultimate had been reached by annealing until a smoother surface was created by further mechanical polishing.

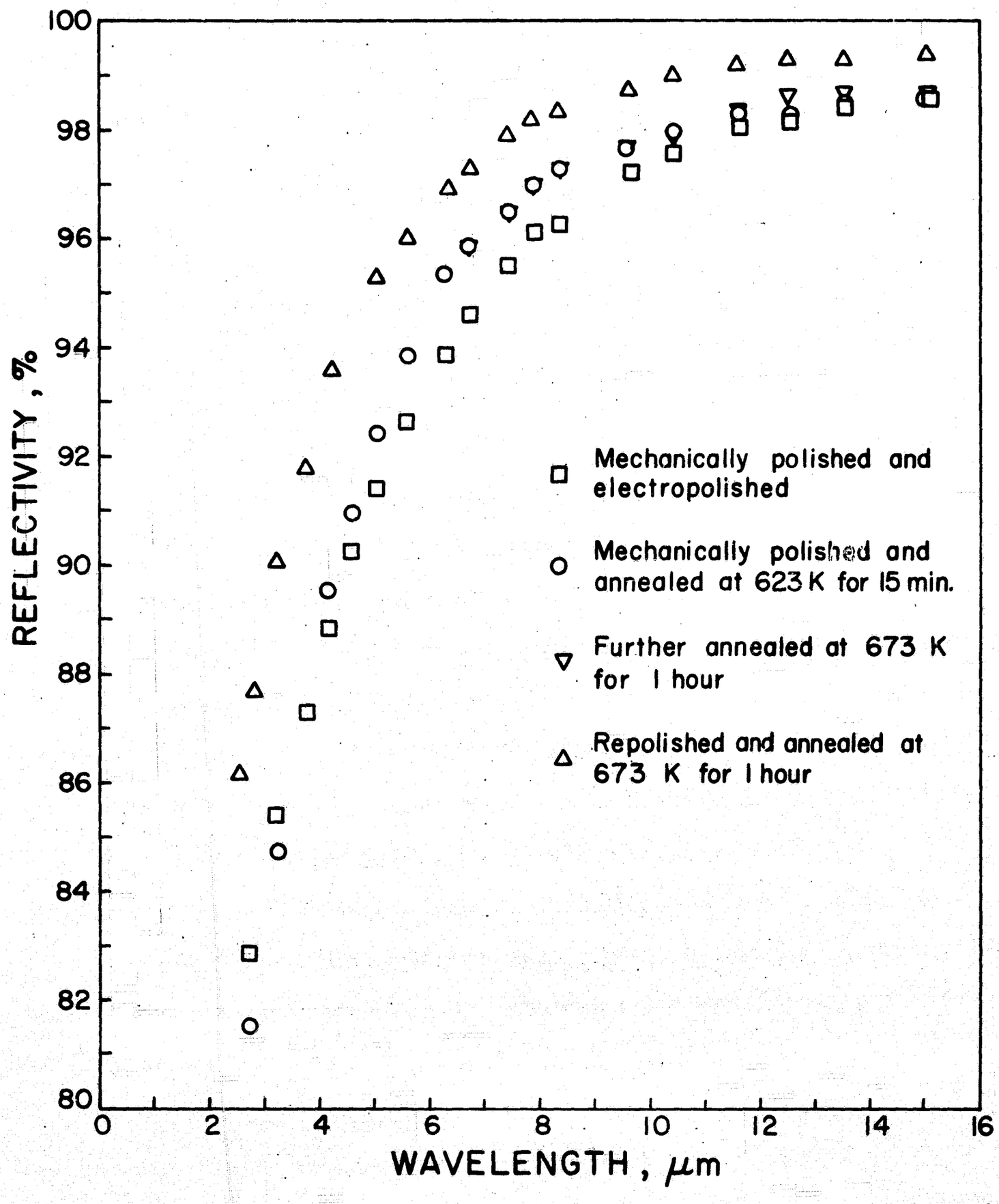

Figure 1. Reflectivity of Nickel Relative to Gold for Different Surface Preparation Procedures

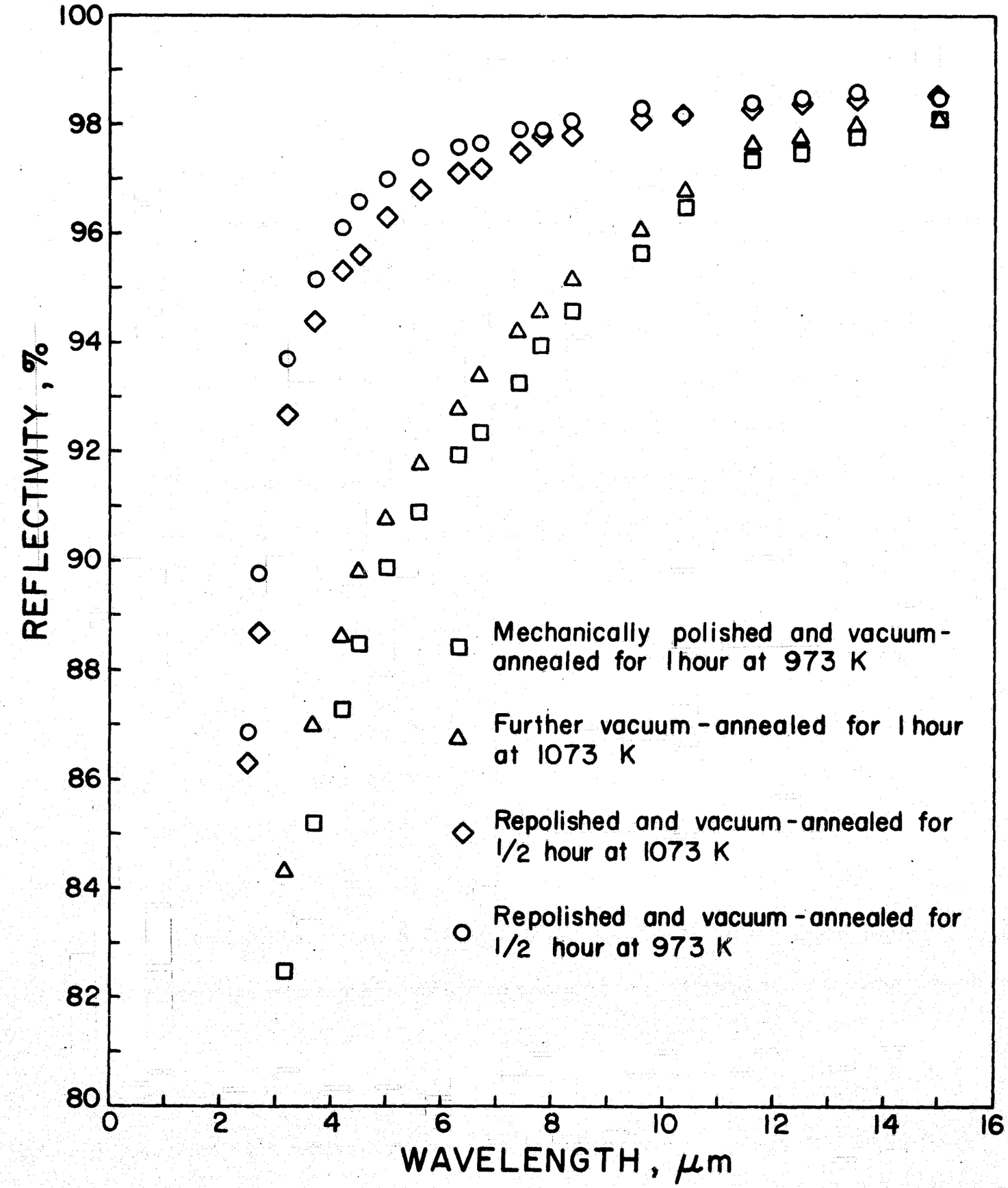

Figure 2. Reflectivity of Platinum Relative to Gold for Different Surface Preparation Procedures

The reference sample was produced by vapor deposition of 99.999% pure gold at 300 Å per second in a vacuum of 8×10^{-6} torr. The total thickness was 1500 Å and was applied on a flat glass substrate which had been precoated with a 70 Å film of nichrome for improved adherence. This sample was selected over several others of similar thickness which had been deposited at higher vacuum (10^{-8} torr) but at lower deposition rates (1 to 16 Å/sec.) since its reflectivity at both 2.5 and 4.0 μm was higher when compared with them at room temperature in the apparatus described below. The absolute determination of the room temperature absorptivity of the gold reference sample at selected laser frequencies is described in section 4.

3. Experimental Apparatus and Procedures

3.1 Optical and Electronic Components

A commercial grating spectrophotometer was used having a nominal wavelength range from 1-700 μm. For these measurements the instrument was fitted with reflectivity optics which direct the source energy upwards onto the inverted horizontal sample at an angle of incidence of less than 9°. A plan of the spectrophotometer with reflectivity optics and cryostat incorporated is shown in figure 3. The sample is positioned at a conjugate image point of the monochromator entrance slit. The source used was a globar throughout; the detector was a

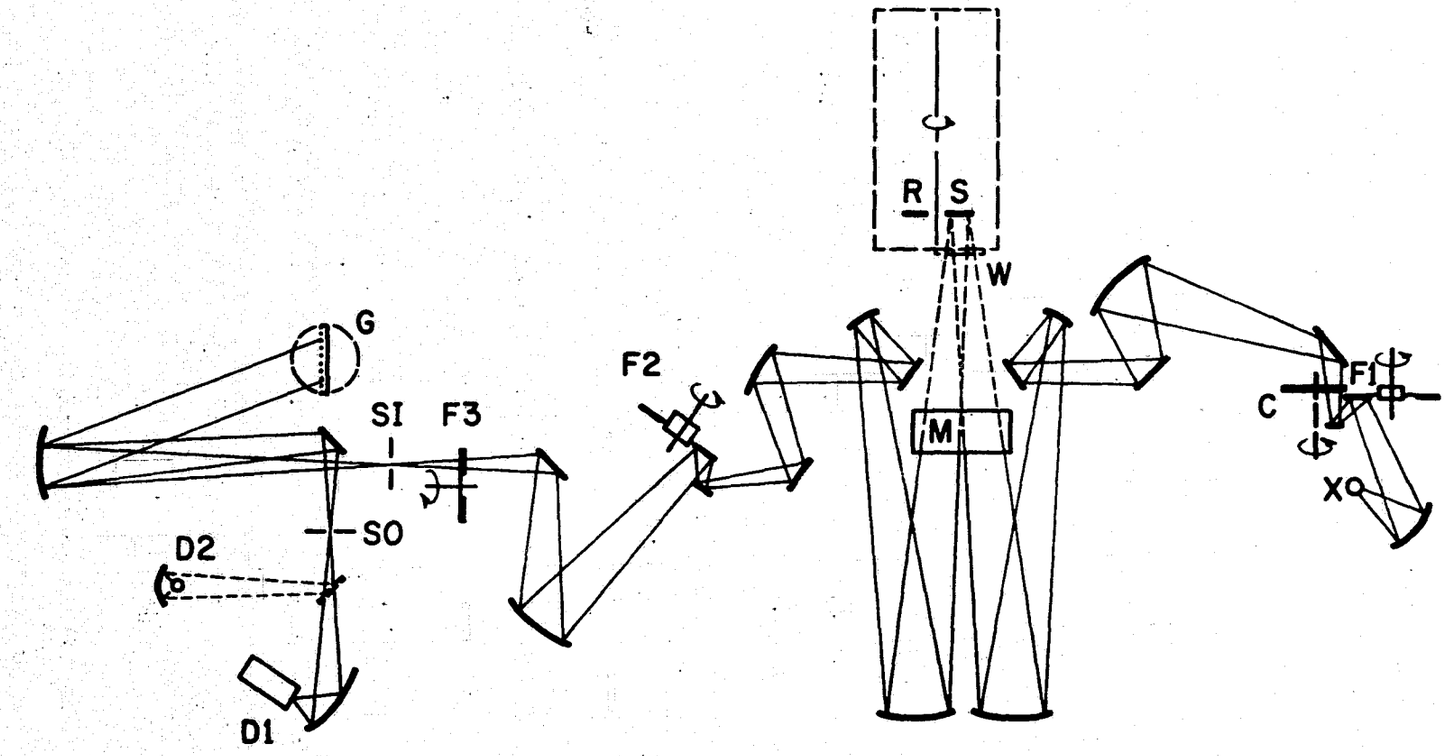

KEY:

C - CHOPPER
D1 - GOLAY CELL DETECTOR.
D2 - THERMOCOUPLE DETECTOR.
F1, F2 - SELECTABLE RESTSRAHLEN FILTERS OR PLANE MIRRORS.
F3 - INTERFERENCE TRANSMISSION FILTERS.
G - INTERCHANGEABLE DIFFRACTION GRATINGS.
M - 45° PLANE MIRROR
R - REFERENCE MIRROR
S - SAMPLE MIRROR
SI - INLET SLIT
SO - OUTLET SLIT
W - CRYOSTAT WINDOW
X - SOURCE

Figure 3. Optical Plan of Spectrophotometer and Reflectivity Optics with Cryostat Incorporated

thermocouple at wavelengths up to 15 μm and a Golay cell for longer wavelengths. The detector signal was amplified by a lock-in amplifier, the reference signal for which was taken from a breaker on the chopper shaft. The amplified signal was read out to four significant digits on a digital voltmeter.

3.2 The Cryostat

For both room and low temperature measurements the sample was mounted in the stainless steel cryostat shown in figure 4. This cryostat was a modified form of one described previously.[19] In the earlier version both sample and reference were held at the same temperature while here the reference was maintained at all times at room temperature.

The cryostat was designed specifically for these measurements. The requirements were to be able to position the reference in the appropriate plane of the spectrophotometer, then, after recording the signal for a few minutes, to replace it quickly with the sample in precisely the same plane while maintaining at all times a high vacuum around the sample. Interchanging sample and reference was effected by rotating the entire inside contents of the cryostat (i.e. the liquid helium vessel B and the liquid nitrogen radiation shield C) by means of the handle H and reduction gears I and J. This turned the collar E which rode on the ball-race F and was sealed to the stationary outer jacket of the

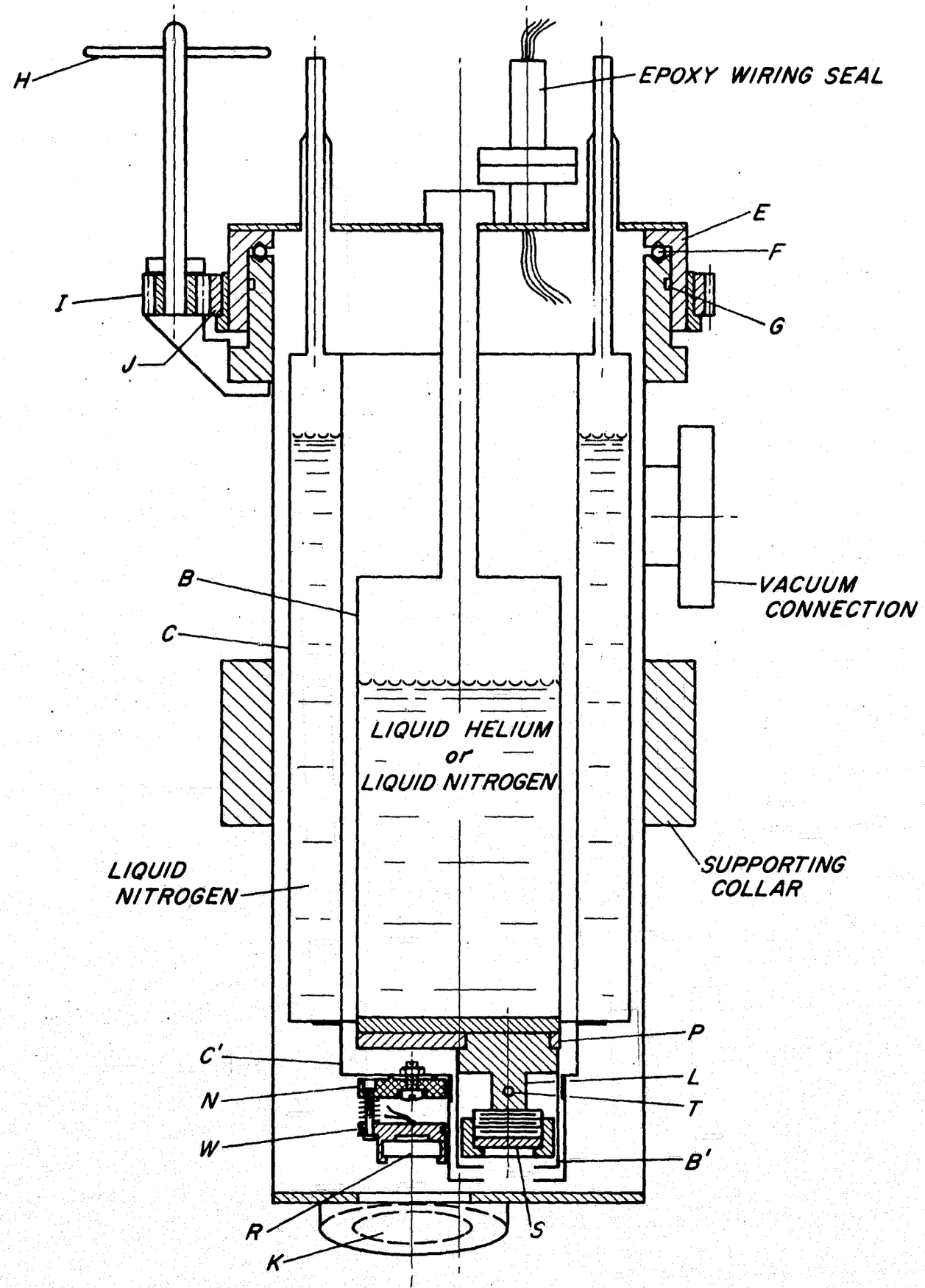

Figure 4. Cryostat

cryostat by the "O" ring G. It was then possible to position either the sample S, or the reference R over the cesium iodide window K through which the spectrophotometer beam entered and left. The window K was inclined at 14° to the horizontal to prevent energy reflected from the window surface from arriving at the monochromator slit. Corrections to the sample plane were achieved by tilting and raising or lowering the whole cryostat, which was supported in the spectrophotometer by a heavy aluminum collar attached to which were three legs resting on the spectrophotometer housing. The legs terminated in screws with which the predetermined adjustment was made. (see 3.4)

The high vacuum required was obtained by use of an ion pump of 8 liters/sec pumping speed attached directly to the cryostat vacuum jacket. With it a vacuum of 5×10^{-8} torr could be maintained throughout low temperature experiments even while interchanging sample and reference. An added advantage of an ion pump is that sample contamination through backstreaming of pump oils is not a problem and there is no need for an intervening cold trap.

The entire cryostat assembly in position in the spectrophotometer can be seen in the photograph, figure 5. The supporting collar, legs, and adjusting screws are clearly evident.

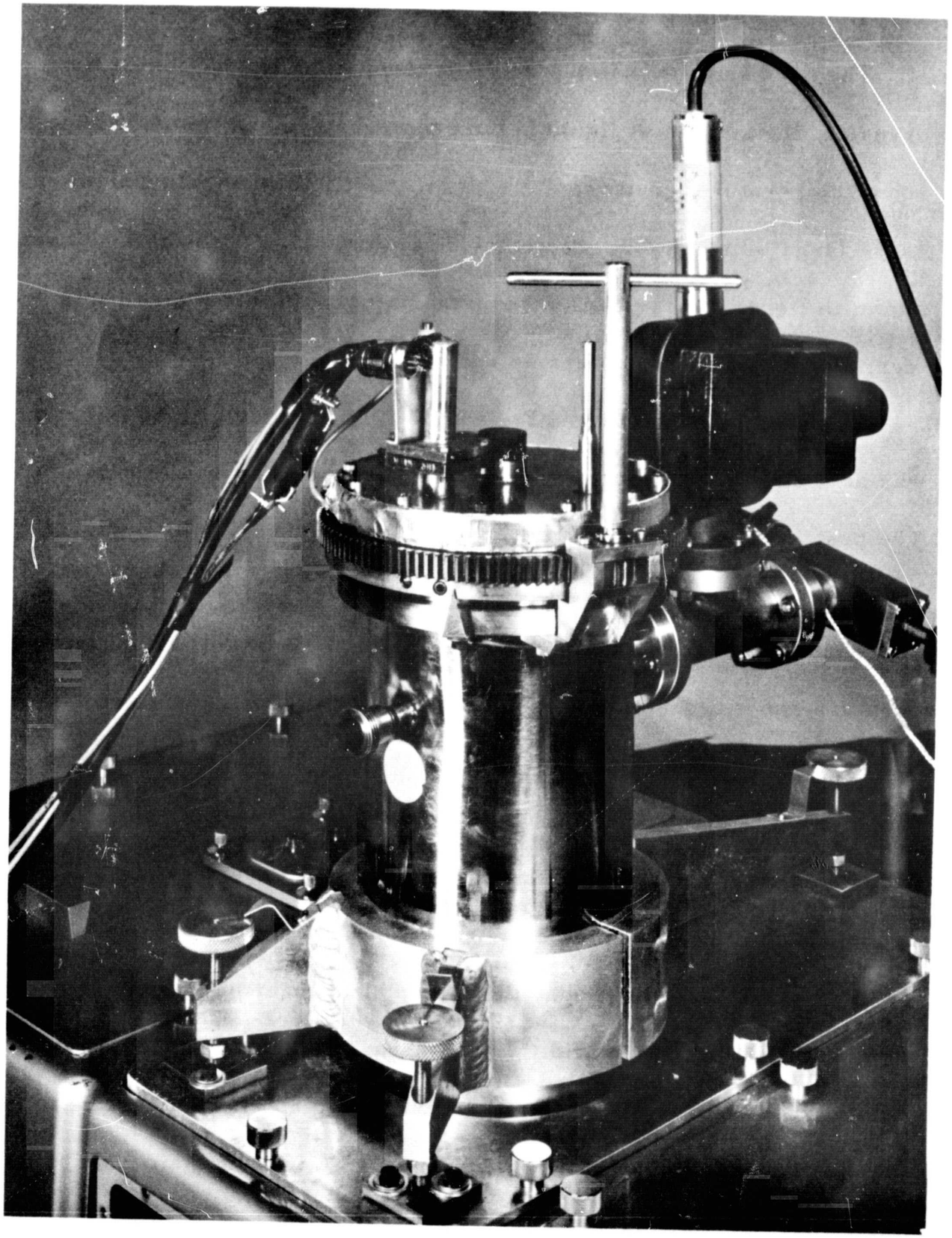

Figure 5. Photograph of Cryostat Installed in Spectrophotometer

3.3 Sample Mounts

The need to place sample and reference side by side inside the cryostat, the sample at liquid helium temperature and the reference at room temperature, presented a somewhat difficult design problem because large temperature gradients were inevitable. The arrangement shown in figure 6 was used in this experiment. In this figure parts are identified by the same letters as in figure 5.

The sample S to be investigated had its back side ground flat and was held against the copper post L, also ground flat, by a screw cap. The post L was silver soldered into the copper plate P which was screwed to the copper base of the helium vessel. The sample was surrounded by a gold plated radiation shield B' at liquid helium temperature and a second one C' at liquid nitrogen temperature except for an aperture to permit entry and exit of the spectrophotometer beam. The sample temperature could be measured by the thermometer T which was a germanium resistance thermometer inserted into a hole in the post L. The thermometer leads were well tempered around L.

The reference was mounted on the platform formed by the nitrogen temperature radiation shield C'. It was in the form of a coated glass plate held in a brass slide mounted by three spring loaded screws to the intermediate nylon platform N. This in turn was held against C' by a single nylon screw, the area of contact being kept to a minimum by two

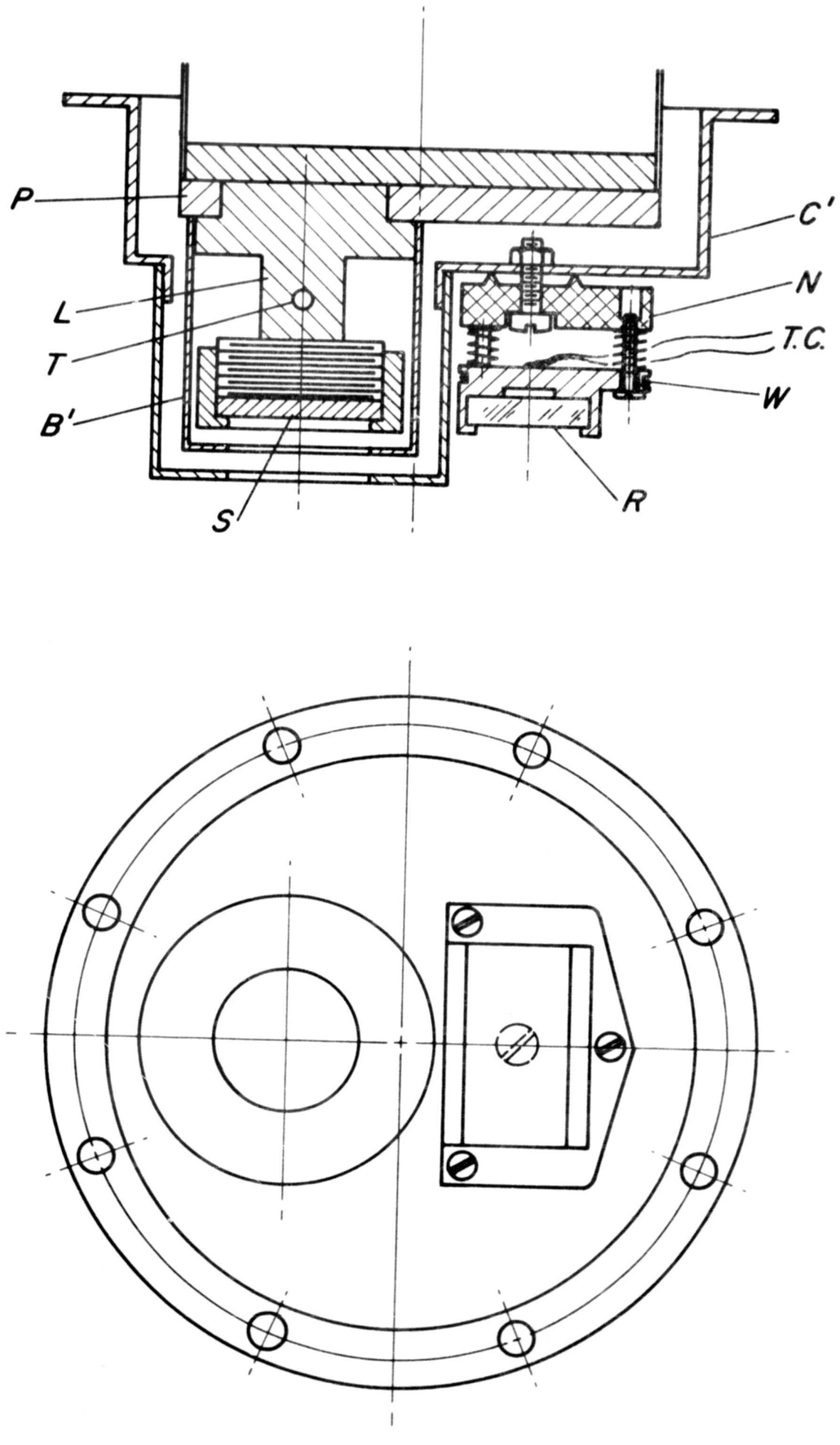

Figure 6. Details of Sample Mounts

knife edges machined on the nylon. By these means good thermal isolation from C' was maintained while at the same time the reference was sufficiently rigidly supported for optical purposes. The reference was maintained at room temperature by the electrical heater W, wound on the brass slide, with current from a controller driven by the error signal of the thermocouple T. C. which was varnished to the back of the slide and well tempered to it.

3.4 Alignment Procedure

Replacing the reference by the sample in precisely the same plane required a preliminary procedure by which the settings of the adjusting screws of the cryostat were determined for both reference and sample in position. It was found that the settings depended somewhat on the temperature of the sample, but for liquid helium temperature it was determined that the alignment procedure could be performed at liquid nitrogen temperature.

The procedure began by setting the mounting screws of the reference such that without any correction to the inclination of the cryostat the sample was approximately in the same plane as the reference on rotating the inside of the cryostat. The reflectance optics were then removed and replaced by a plane mirror inclined at 45° so that the sample or reference could be viewed through the window K. The required correction to the settings of the adjusting screws when the

sample was brought into position were then determined by autocollimation with the aid of a cathetometer telescope and illuminated cross-hairs as illustrated in figure 7. The adjusting screws were fitted with pointers which enabled precise repositioning of the cryostat for the experimental run. The adequacy of the procedure was checked by comparing the signals from two gold samples at room temperature. These samples had been produced simultaneously side by side in a vapor deposition apparatus. They were found to give identical signals. In fact it was found that the tilt correction as described above could be determined to considerably greater precision than was required to avoid error in the relative reflectivity of a sample.

3.5 Data Recording Procedure

Data reading was relatively straightforward once the sample and reference were mounted, the cryostat evacuated and cooled to liquid nitrogen temperature, and the alignment procedure completed. The spectrophotometer was allowed to warm up for several hours and a steady flow of dry nitrogen gas through the spectrophotometer was put into effect about 1 hr. before an intended run to reduce the water vapor concentration. When the detector signal appeared to be steady the cryostat was cooled down further by transfer of liquid helium. For room temperature runs the helium vessel was filled with trichlorofluoromethane in order to stabilize the temperature. Reflectivity data were taken point

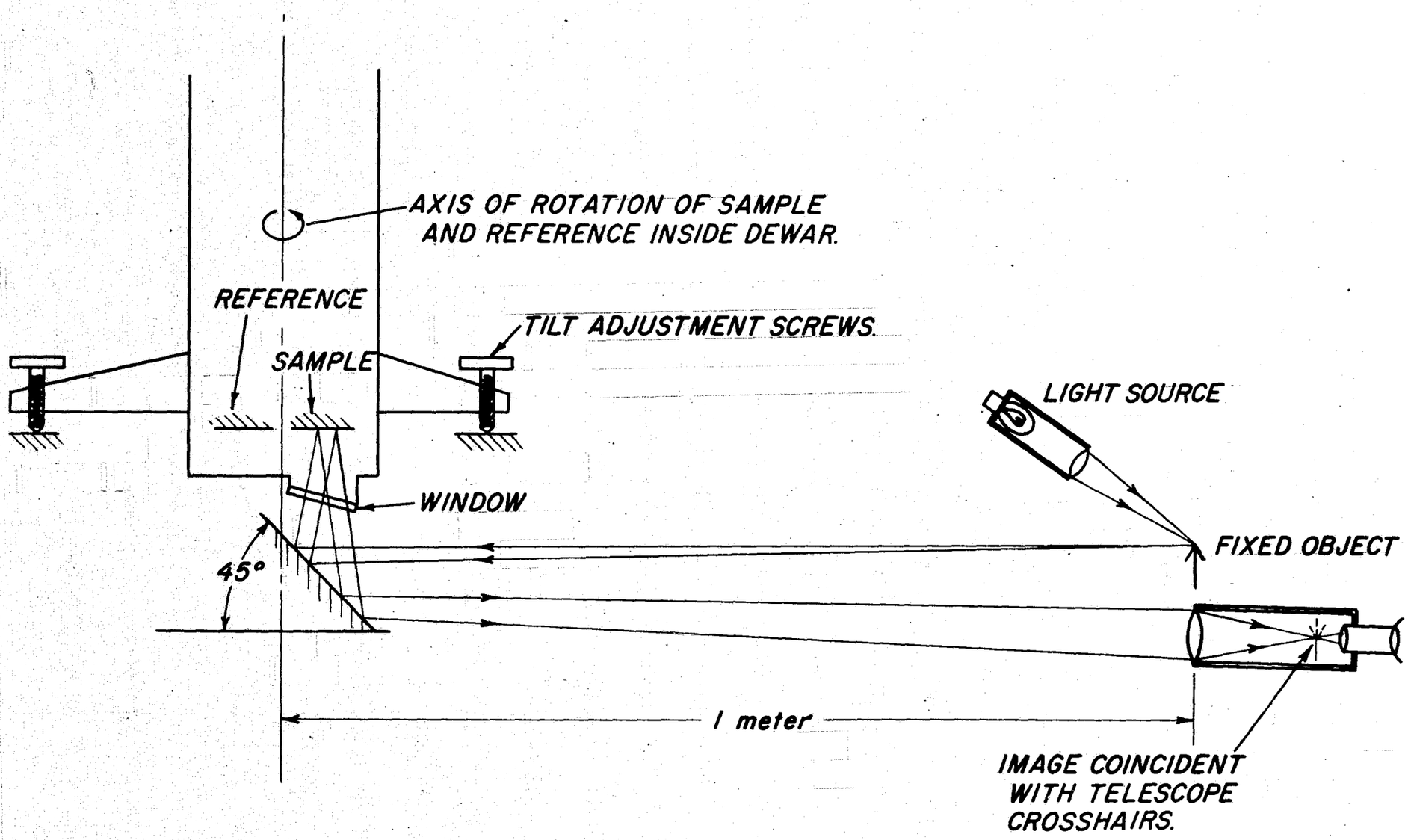

Figure 7. Illustration of Alignment Procedure

by point rather than by scanning, since in this way the reference signal could be checked immediately before and immediately after the sample signal to determine if any signal drift had taken place. The signal in each case was observed for a few minutes after becoming steady with a filter time constant of 30 or 100 sec to average out noise. In this way repeatability of the relative reflectivity could be held to ± 0. 1% at short wavelengths to ± 0. 2% at the longer wavelengths. Points were discarded if the reference signal recorded after the sample signal had drifted from its initial value by more than this amount. This criterion set the upper wavelength limit to the data taken with the spectrophotometer, since for wavelengths greater than about 50 μ m no such signal stability could be obtained.

In addition to sample and reference signal the true instrument zero was recorded at each amplifier gain, since, particularly with the Golay cell, a spurious signal due to chopper vibrations often accompanies the optical signal.

With the procedure outlined, the relative reflectivity of the sample could be determined at a particular wavelength in about 5 minutes. One charge of liquid helium (1 liter) permitted 3 to 4 hours of operation.

4. Determination of the Room Temperature Absorptivity of the Gold Reference Mirror

4.1 Laser Calorimeter

For the measurement of the absorptivity of the gold reference mirror a calorimeter was built for use with infrared lasers that were available. These lasers were:

i) A CO_2 laser having a strong emission at 10.6 μm. This laser has been described many times in the literature[24] and is probably the most intense known for a given size. The particular one used here was 0.5 m in length and had a power output through a germanium window of about 2W concentrated in a beam of parallel radiation of 3mm diameter. An iris was used to reduce the energy to about 100 mW.

ii) An H_2O laser[25] with its strongest emission at 28.0 μm and less intense emissions at 78.5 and 118.8 μm. A power output of about 100mW was available at 28.0 μm, but insufficient power was available in the weaker lines for use in these measurements. This laser was 8 m in length and had a diameter of 80 mm. The radiation emerged through a polyethylene lens with a focus at 200 mm. For

these measurements a collimated beam of about 3 mm diameter was produced after passing through a second lens of 24 mm focal length.

iii) An HCN[26] laser with a strong emission at 337 μm and a weak emission at 373 μm. Again only the stronger emission was of suitable power, namely 50 mW. This laser was also 8 m in length and was 150 mm in diameter. Similar polyethylene lenses were used to produce a parallel beam of 3 mm in diameter.

The calorimeter itself is illustrated in figure 8. The laser beam could either be absorbed on the gold mirror, which was cemented on the outside of a thin spherical copper shell (0.10 mm thickness), or it could be absorbed inside the shell by rotating with the plastic knob to place a small inlet cone in the beam. The copper shell and cone were painted inside with 3 coats of a flat black paint known as NEXTEL*; the shell was gold plated on the outside. In an intermediate position the laser beam impinged on a smallcopper plate cemented to the shell and coated with NEXTEL in the same manner as the shell interior. With this the absorptivity of the paint could be determined for use in assessing

* Minnesota Mining and Manufacturing Co.

Thc use in this paper of trade names of specific products is essential to a proper understanding of the work presented. Their use in no way implies approval, endorsement, or recommendation by NBS.

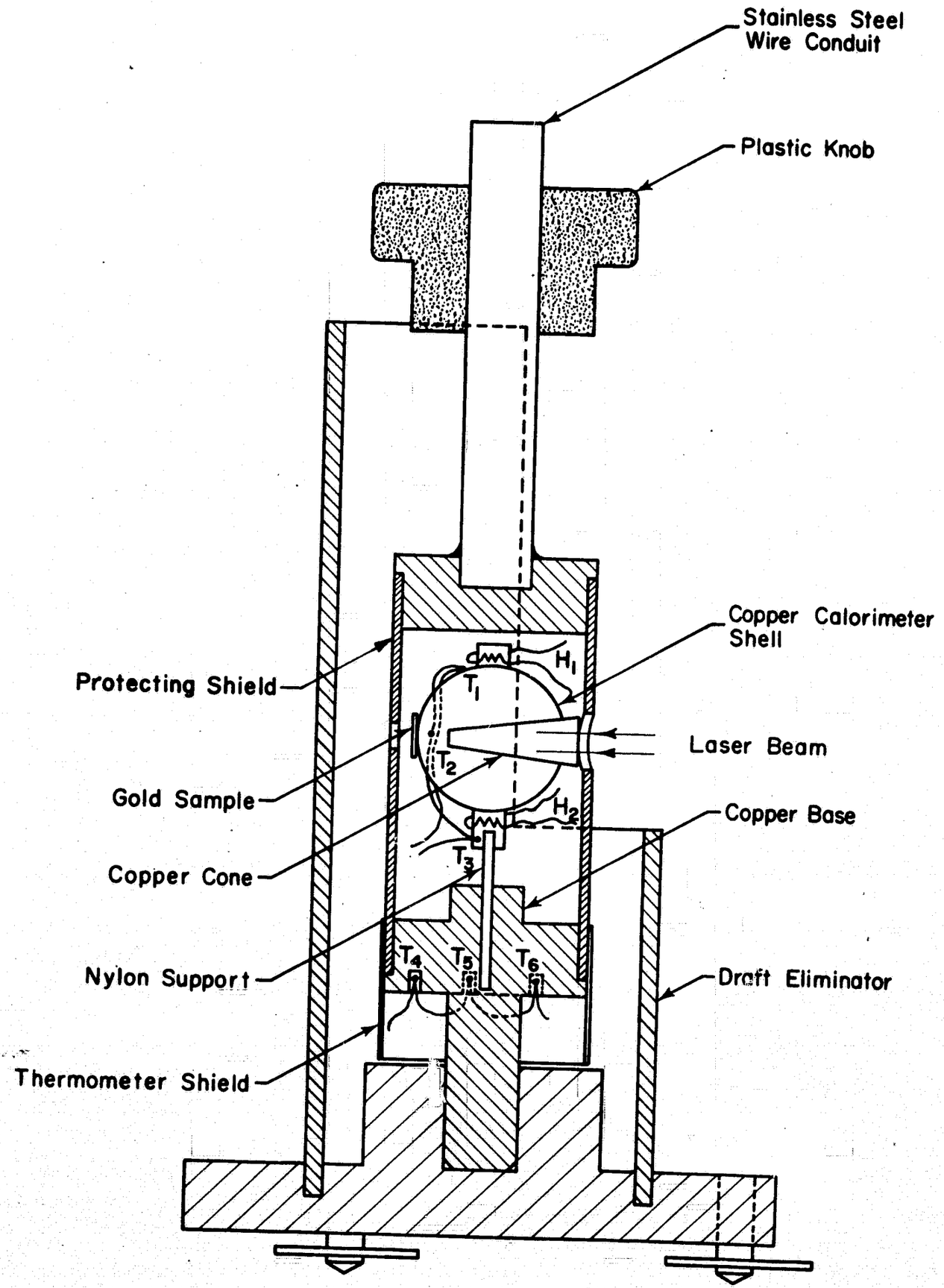

Figure 8. Laser Absorptivity Calorimeter

the absorption efficiency of the shell cavity.

The calorimeter shell was supported by a nylon pin mounted in a copper base. Except for holes to permit entry of the laser beam the shell was completely enclosed by a brass protecting shield to keep down perturbations from stray radiation and drafts. A second draft eliminator around this provided additional protection. A shaft on the copper base fitted into an aluminum base and permitted rotation of the calorimeter without disturbing its position relative to the laser optics on an optical bench. By setting the plastic knob off from the calorimeter with a length of stainless steel tubing, this could be done without serious temperature perturbations from the hand.

When a steady temperature difference exists between the calorimeter shell and base this difference is an indication of the power being absorbed. The shell temperature was indicated by three thermistors T_1, T_2, and T_3 connected in series; two were cemented to the shell and one just at the point where the nylon pin was attached. In this way an average shell temperature was indicated. Three similar matched thermistors T_4, T_5, and T_6 in series also were cemented in holes in the copper base. A thin aluminum shield protected these from direct impingement by stray radiation. Each set of three thermistors formed one arm of a bridge which could be balanced when the shell and base had come to thermal equilibrium. In order to calibrate the calorimeter

two heaters H_1 and H_2, in the form of 1/8 W carbon radio resistors, were cemented in holes, the first in a brass boss soldered to the top of the shell and the second in a hole in a similar boss at the base of the shell; the latter served also to attach the nylon pin. In this way the calorimeter could be tested to ensure that its response was independent of the point at which power was absorbed on the shell. The calibration is represented in figure 9 by a plot of the reciprocal of the responsivity in mW/mV versus the bridge signal at 5 minutes after start when the bridge was driven by 2.000V.

The calorimeter illustrated was in fact a second model with many improvements incorporated on the basis of experience with a prototype. These include the use of multiple thermistors, the inlet cone, the thermometer shield, a lighter shell, and the NEXTEL paint which was far superior to a black copper oxide coating used initially.

Much effort was expended on ensuring that substantially all the beam radiation could be absorbed in the shell. This is the more difficult the longer the wavelength of the radiation because almost every coating known becomes less black the longer the wavelength. In developing the final design the power indicated by the calorimeter was frequently compared with that indicated by a faster responding but less sensitive power meter developed at the National Bureau of Standards specifically for infrared laser power measurements. In the final design the powers

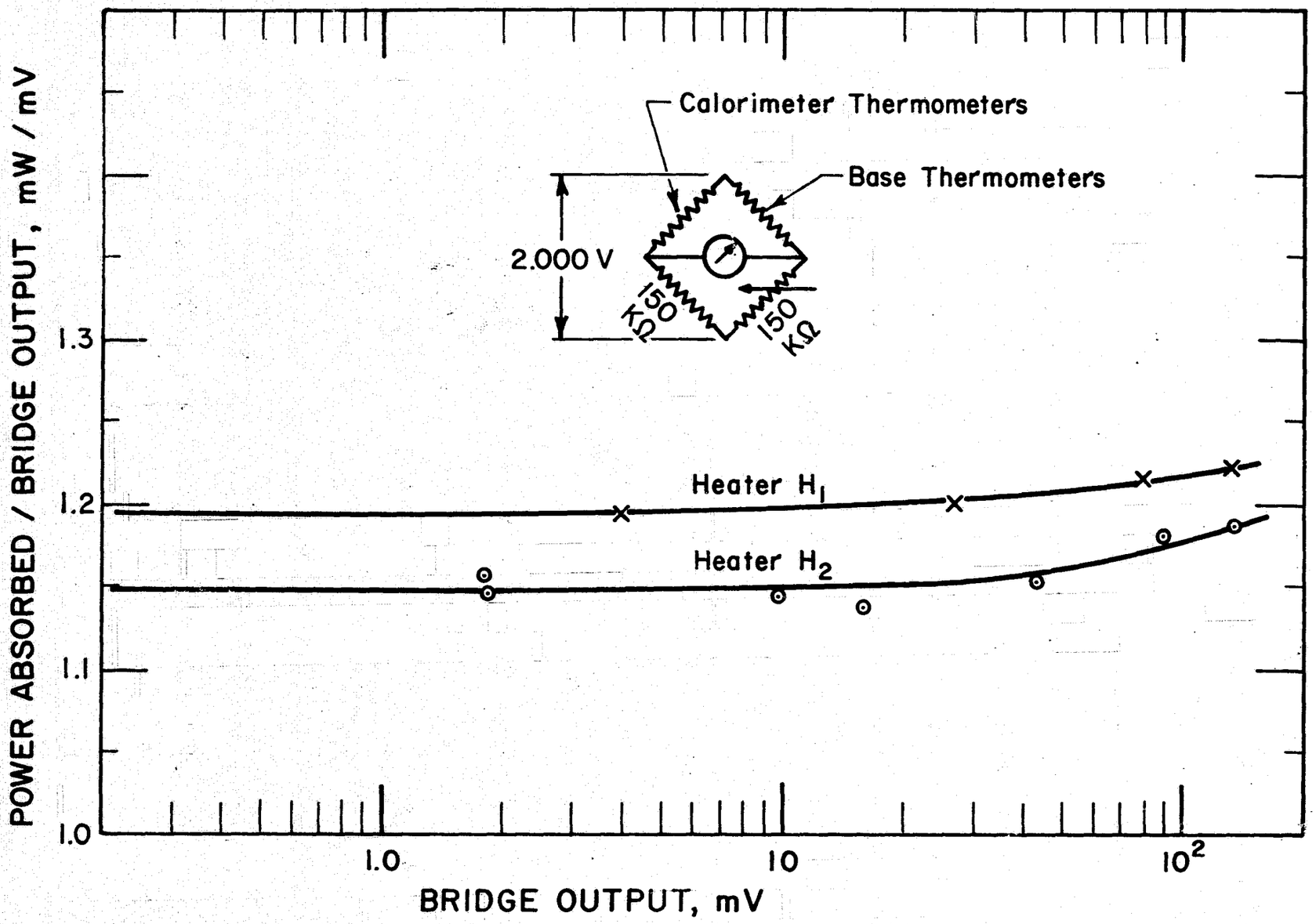

Figure 9. Calibration of Calorimeter

indicated by the two instruments were always within 5% of each other and no trend with wavelength was observed which, on account of the wavelength dependence of the paint, might have indicated a serious departure from blackness.

Based on a simple spherical cavity without the cone and on the measured ratio of power absorbed by the paint to that absorbed by the cavity, a lower limit of 99.3% can be set for the cavity absorption efficiency at 337 μm. Now the use of the cone can only enhance this efficiency because it is truncated short of the point at which an extreme axial ray would be turned back after multiple reflections; it provides a strongly divergent beam inside the cavity and, being set off axis, no specular ray could be reflected straight back out again after encountering the shell wall. It is therefore firmly believed that, to an accuracy of a few percent, the cavity can be assumed to be black and no systematic correction needs to be applied in data reduction on this account.

Some of the important calorimeter parameters were as follows:

Time constant	2 min.
Responsivity	0.83 to 0.87 V/W
Detectivity	0.05 mW
Temperature rise	0.022°C/mW

In making measurements the calorimeter was placed on an optical bench on which the laser rested and was set relative to the laser outlet optics such that the beam was centered on sample or cavity after passing through a stop of smaller diameter than the framing aperture of the protective shield. Heat sensitive paper was used in all cases to locate the beam and center it. When directed onto the gold sample the reflected beam was also located and the angle of incidence carefully chosen so that the reflected energy was frustrated by the stop. The beam reflected from the stop was also directed away from calorimeter.

After allowing the calorimeter to come to equilibrium laser power was admitted by opening a shutter. Readings of the out-of-balance of the bridge were taken with time and, instead of waiting for steady state to be achieved, the power was determined from the reading at 5 minutes after start, as had been done for calibration also. With the time constant stated this was sufficient to achieve 92% of the steady state reading and was short enough on the other hand to minimize the contribution from long term drift.

4.2 Calorimeter Results

The absorptivity of the sample was calculated as the ratio of the power absorbed when the laser beam impinged on the sample to that when it was absorbed in the cavity. The results for the gold and the NEXTEL paint are given in Table 1. For the gold each value represents

Table 1. Results of Room Temperature Measurements of Absorptivity with Laser Calorimeter.

wavelength μ m.	absorptivity of gold	uncertainty	absorptivity of NEXTEL
10.6	0.0116	±0.0008	0.89
28.0	0.0139	±0.0009	0.96
337	0.0111	±0.0011	0.67

Average absorptivity of gold reference mirror 0.0127

an average of several observations. The accuracy of the results is governed by the departure of the cavity from 100%, but more serious was the problem of repeatability. This arose from the long term drift of the calorimeter, which was particularly important for observations on the small power absorbed by the gold (of the order of 1.0 mW). Usually, after an hour's time for equilibrating, the drift of the out-of-balance signal of the bridge could be held to within 10 μV in 5 minutes, which corresponded to about 0.01mW, or 1% of the power absorbed by the gold; however no assurance could be gained that within the duration of an observation the drift remained at this level. The observed repeatability was from ± 7 to ± 10%.

The results are a little surprising in that the absorptivity of the gold at 28.0 μm is higher than at 10.6 μm; the Drude theory could not be fit to these data by any choice of material parameters. This

anomaly is not important as regards reduction of the transition metal data to absolute absorptivities because the shift implied is within the precision of those data. To the accuracy required it is sufficient to treat the gold absorptivity as constant in the wavelength range from 2.5 to 50 μm and thus a mean value of 0.0127, or 0.9872 for the reflectivity, was assumed.

In comparing these results with those of other workers it is seen that they confirm the findings of Bennet and Ashley[17] that the deposition vacuum is all important for lowest absorptivity. Thus, in the region of essentially constant absorptivity Bennet and Ashley found a value of 0.0060 for samples deposited at 10^{-9} torr, while the optical constants of Padalka and Shklyarevskii[27] imply a value of 0.0106 for samples deposited at 10^{-5} torr in good agreement with the present data.

5. Experimental Results

5.1 Data Reduction and Presentation

Let Y_s and Y_g be the digital voltmeter readings for sample and reference respectively and let Y_o be that obtained with the beam blocked. Let A_g be the absorptivity of the gold reference. Then the absorptivity of the sample A_s is given by the data reduction formula:

$$A_s = 1 - (1 - A_g) \cdot \frac{Y_s - Y_o}{Y_g - Y_o} .$$

The results for the absorptivities of the nickel, iron, platinum and chromium samples are given respectively in figures 10, 11, 12 and 13 plotted versus wavelength in μm. The results are tabulated in Tables 2 to 5. The curves shown in the figures were calculated from theory and will be discussed in section 6.

5.2 Experimental Errors

The precision of the data is determined by instrument drift and was held to ± 0.1% in reflectivity below 15 μm and to ± 0.2% between 15 and 50 μm.

Systematic errors arise from the non-linearity of the detector-amplifier-digital voltmeter system and from spectral impurity of the spectrophotometer. The former has been checked by measuring the transmittances of dielectric slabs individually and in pairs. The product of individual transmittances was found to be within 0.3% of the transmittances measured in pairs.

The spectral purity is a function of wavelength and is primarily due to imcomplete filtering of higher order radiation; the monochrometer operates in first order. This affects the measured value of reflectivity only insofar as sample and reference differ in reflectivity at the wavelength in question and at the wavelength of the higher order stray radiation. Thus taking the manufacturer's specification of less than 1% stray radiation and assuming it to be entirely second order,

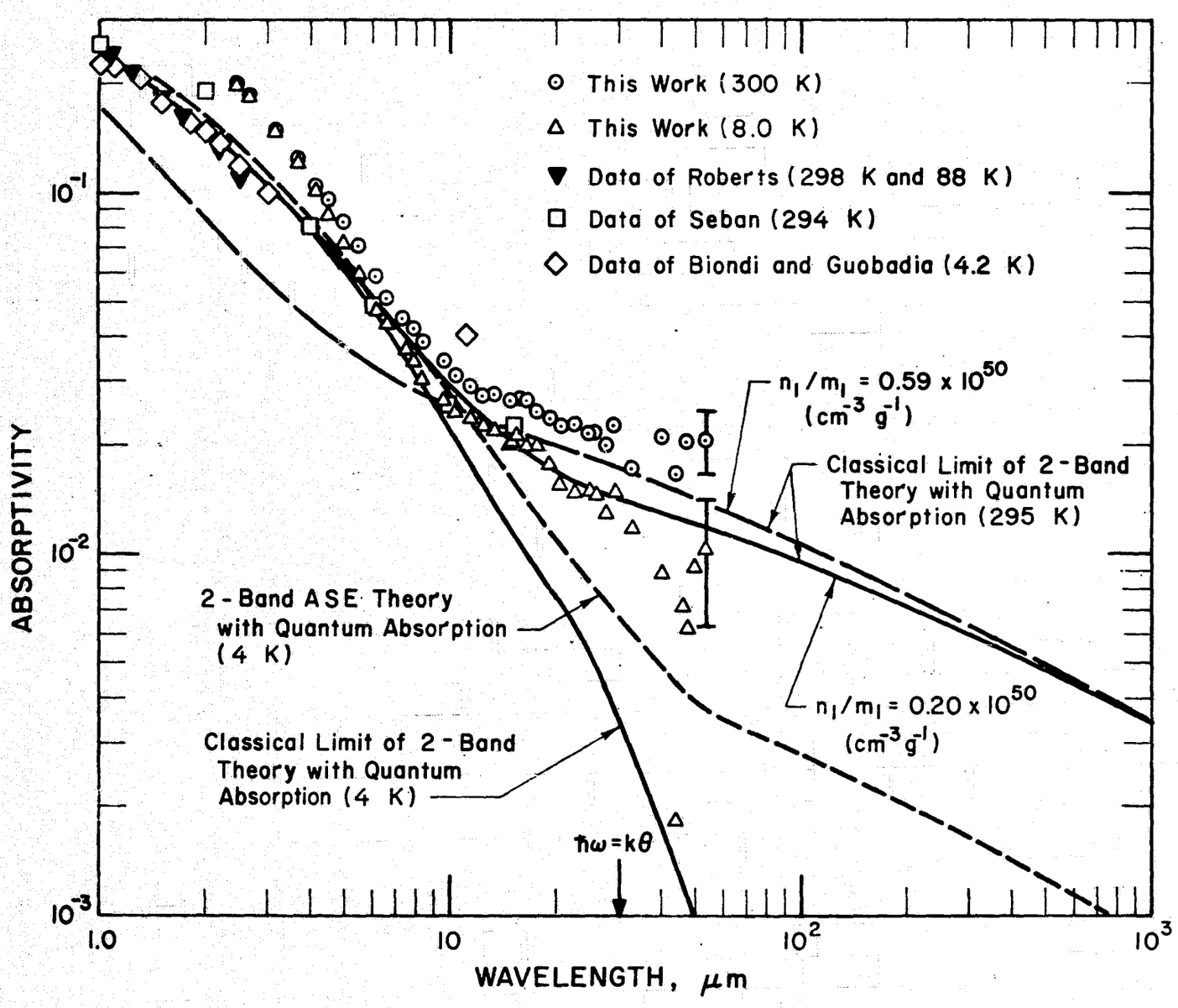

Figure 10. Comparison of Experimental and Calculated Absorptivities of Nickel

Table 2. Absorptivity of Nickel Sample

300 K		8.0 K	
Wavelength (μm)	Absorptivity	Wavelength (μm)	Absorptivity
2.48	0.2000	2.48	0.1987
2.68	0.1851	2.68	0.1821
3.21	0.1508	3.21	0.1481
3.68	0.1270	3.66	0.1212
4.15	0.1083	4.15	0.1014
4.53	0.0956	4.53	0.0862
4.99	0.0825	4.99	0.0728
5.53	0.0713	5.53	0.0594
6.23	0.0588	6.23	0.0471
6.62	0.0517	6.62	0.0432
7.35	0.0456	7.35	0.0366
7.79	0.0419	7.79	0.0341
8.30	0.0390	8.30	0.0305
9.56	0.0341	9.56	0.0267
10.41	0.0315	10.41	0.0247
11.59	0.0291	11.59	0.0234
12.46	0.0274	12.46	0.0225
13.47	0.0275	13.47	0.0217
14.95	0.0267	14.95	0.0203
14.91	0.0266	14.91	0.0202
15.50	0.0270	15.50	0.0210
16.55	0.0256	16.55	0.0197
17.72	0.0248	17.72	0.0198
19.10	0.0235	19.10	0.0178
20.71	0.0225	20.71	0.0155
22.61	0.0230	22.61	0.0149
24.90	0.0217	24.90	0.0150
26.15	0.0216	26.15	0.0145
27.61	0.0200	27.61	0.0129
29.32	0.0225	29.32	0.0149
33.02	0.0174	33.02	0.0118
40.02	0.0210	40.02	0.0087
44.07	0.0168	44.07	0.0018
47.36	0.0204	46.44	0.0071
53.95	0.0205	47.36	0.0063
		50.50	0.0091
		53.95	0.0102

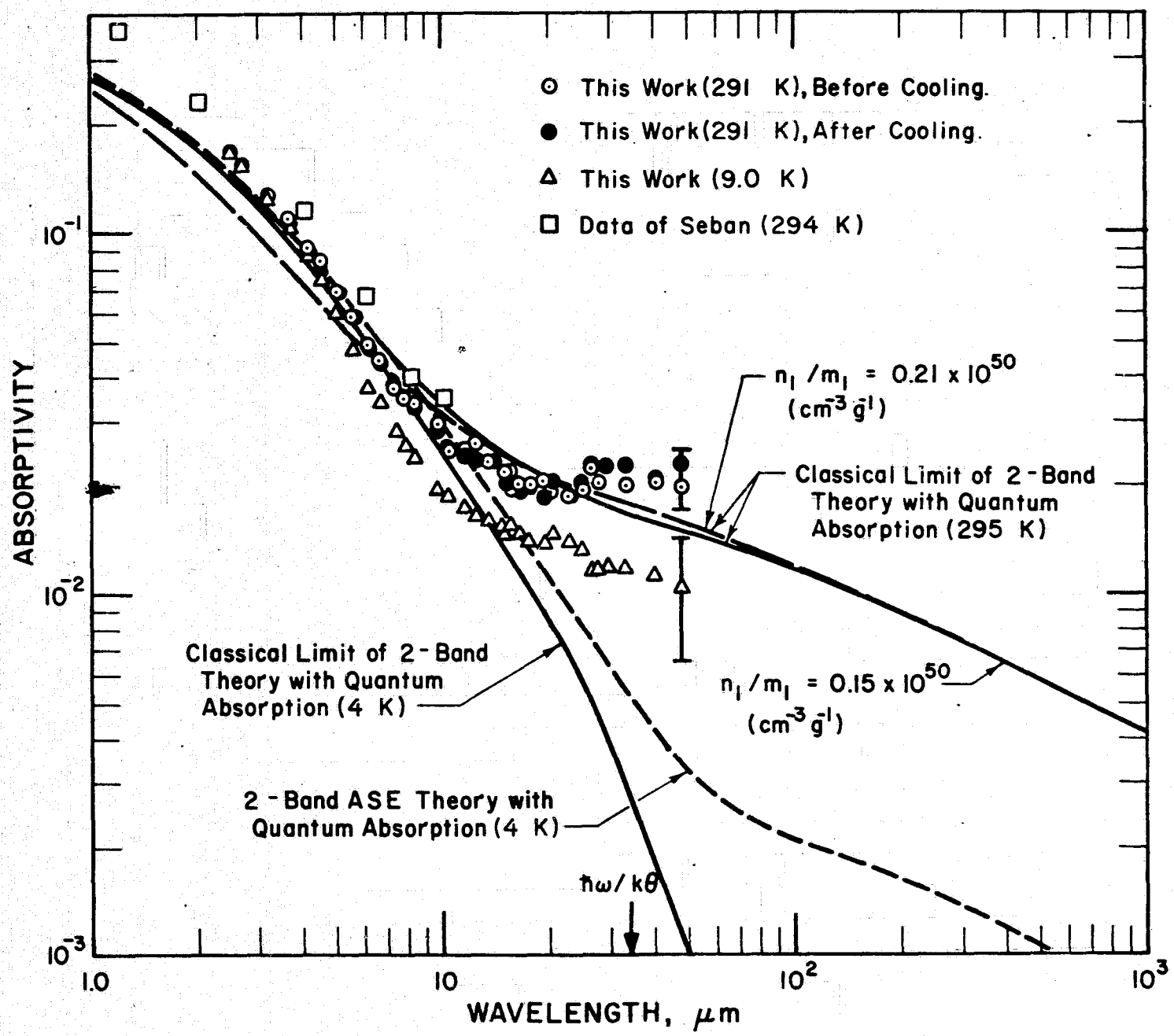

Figure 11. Comparison of Experimental and Calculated Absorptivities of Iron

Table 3. Absorptivity of Iron Sample

Wavelength	Absorptivity at 291 K (Before Cooldown)	Absorptivity at 9.0 K	Absorptivity at 291 K (After Cooldown)
2.48	0.1700	0.1648	0.1668
2.68	0.1580	0.1520	0.1578
3.21	0.1280	0.1247	0.1299
3.68	0.1110	0.1035	0.1092
4.15	0.0913	0.0862	0.0883
4.53	0.0840	0.0739	0.0794
4.99	0.0692	0.0596	0.0691
5.53	0.0583	0.0477	0.0585
6.23	0.0492	0.0375	0.0476
6.62	0.0446	0.0336	0.0439
7.35	0.0366	0.0277	0.0382
7.79	0.0353	0.0256	0.0349
8.30	0.0335	0.0234	0.0333
9.56	0.0288	0.0192	0.0278
10.41	0.0252	0.0186	0.0255
11.59	0.0251	0.0172	0.0246
12.46	0.0260	0.0164	0.0236
13.47	0.0231	0.0159	0.0230
14.95	0.0208	0.0144	0.0198
14.91	0.0216	0.0155	0.0207
15.50	0.0219	0.0153	0.0204
16.55	0.0198	0.0144	0.0190
17.72	0.0196	0.0139	0.0193
19.10	0.0205	0.0138	0.0185
20.71	0.0193	0.0144	0.0202
22.61	0.0185	0.0128	0.0185
24.90	0.0195	0.0133	0.0191
26.15	0.0221	0.0118	0.0225
27.61	0.0201	0.0117	0.0225
29.32	0.0192	0.0118	0.0229
33.02	0.0200	0.0118	0.0223
40.02	0.0204	0.0112	0.0214
47.36	0.0196	0.0104	0.0229

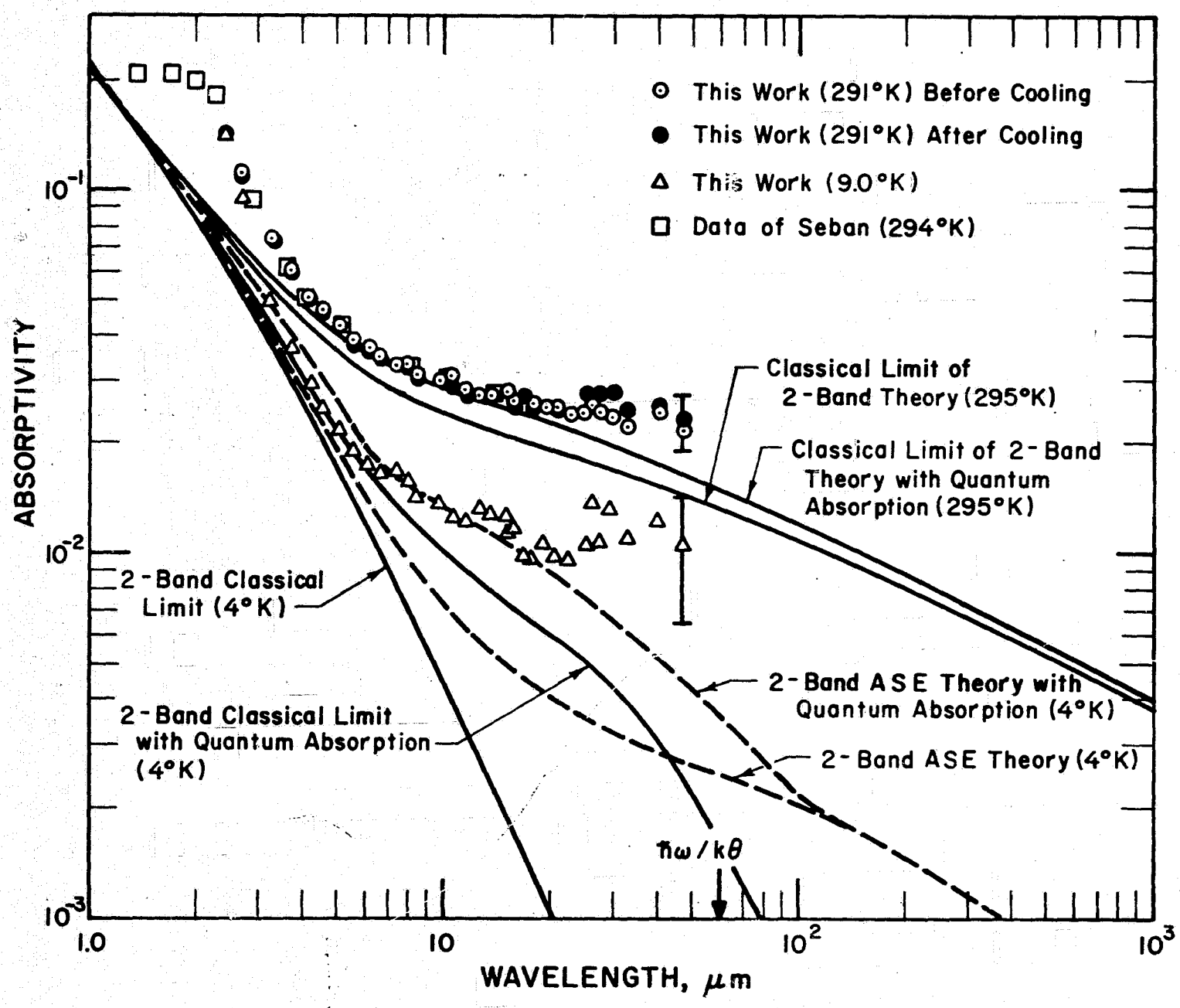

Figure 12. Comparison of Experimental and Calculated Absorptivities of Platinum

Table 4. Absorptivity of Platinum Sample

Wavelength (μm)	Absorptivity at 291 K (Before Cooldown)	Absorptivity at 9.0 K	Absorptivity at 291 K (After Cooldown)
2.48	0.1420	0.1510	0.1401
2.68	0.1133	0.0956	0.1119
3.21	0.0746	0.0494	0.0745
3.68	0.0603	0.0363	0.0593
4.15	0.0510	0.0292	0.0506
4.53	0.0465	0.0248	0.0453
4.99	0.0422	0.0218	0.0418
5.53	0.0388	0.0190	0.0372
6.23	0.0361	0.0179	0.0357
6.62	0.0352	0.0169	0.0344
7.35	0.0333	0.0170	0.0327
7.79	0.0334	0.0159	0.0325
8.30	0.0314	0.0144	0.0302
9.56	0.0300	0.0139	0.0290
10.41	0.0309	0.0123	0.0287
11.59	0.0283	0.0123	0.0269
12.46	0.0277	0.0133	0.0274
13.47	0.0270	0.0128	0.0277
14.95	0.0279	0.0128	0.0275
14.91	0.0260	0.0113	0.0266
15.50	0.0260	0.0118	0.0250
16.55	0.0261	0.0099	0.0265
17.72	0.0255	0.0097	0.0255
19.10	0.0250	0.0107	0.0251
20.71	0.0250	0.0098	0.0243
22.61	0.0241	0.0097	0.0240
24.90	0.0241	0.0107	0.0274
26.15	0.0257	0.0140	0.0268
27.61	0.0242	0.0108	0.0278
29.32	0.0238	0.0133	0.0278
33.02	0.0220	0.0112	0.0247
40.02	0.0241	0.0123	0.0258
47.36	0.0218	0.0108	0.0232

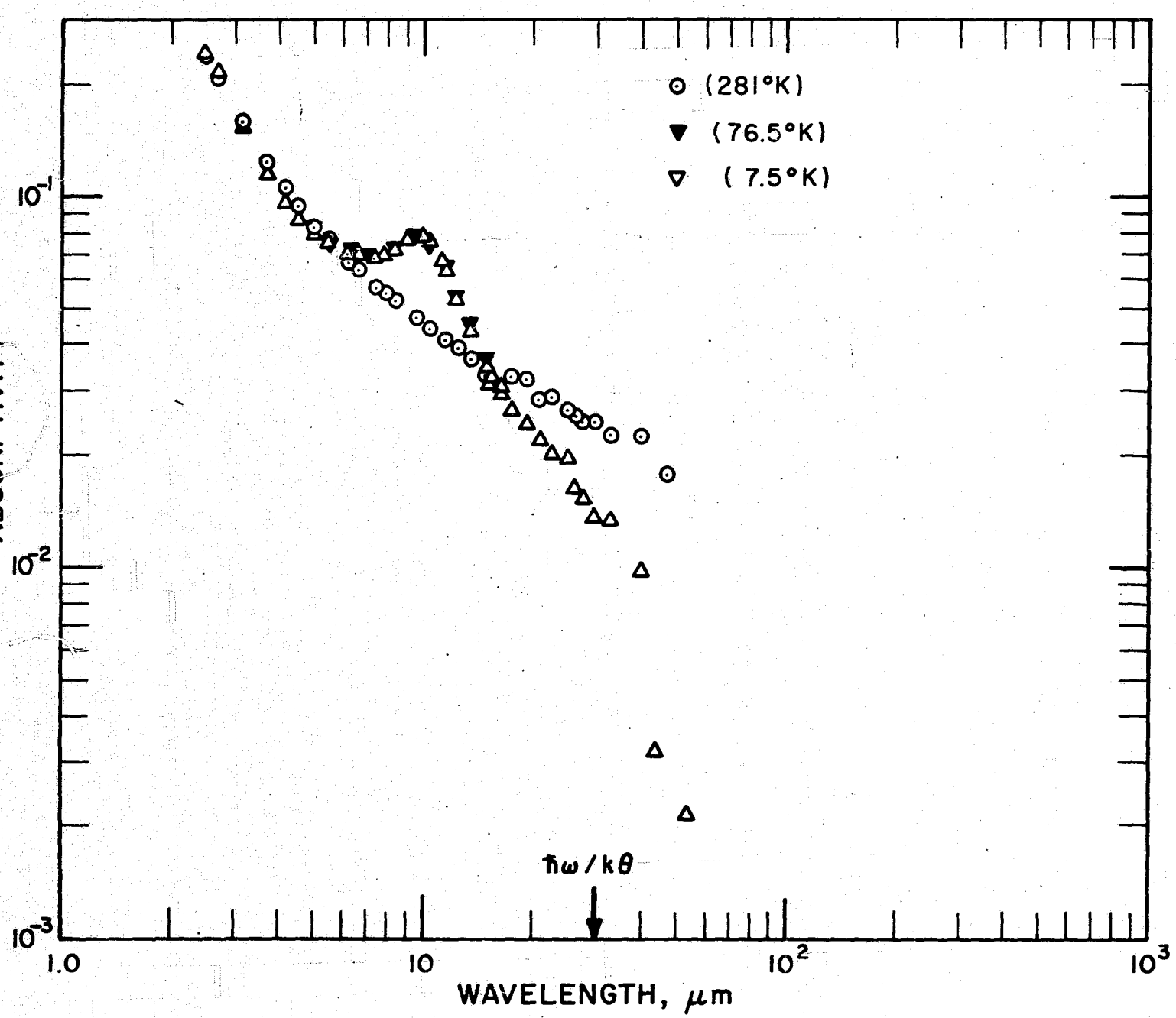

Figure 13. Experimental Absorptivity of Chromium

Table 5 Absorptivity of Chromium Sample

281 K		76.5 K		7.5 K	
Wavelength (μm)	Absorptivity	Wavelength (μm)	Absorptivity	Wavelength (μm)	Absorptivity
2.48	0.2382	4.99	0.0817	2.48	0.2398
2.68	0.2086	5.53	0.0748	2.68	0.2147
3.21	0.1537	6.23	0.0713	3.21	0.1509
3.68	0.1244	6.62	0.0700	3.68	0.1153
4.15	0.1050	7.35	0.0686	4.15	0.0956
4.53	0.0939	7.79	0.0684	4.53	0.0868
4.99	0.0832	8.30	0.0719	4.99	0.0799
5.53	0.0768	9.56	0.0775	5.53	0.0748
6.23	0.0662	10.41	0.0739	6.23	0.0701
6.62	0.0639	11.59	0.0647	6.62	0.0699
7.35	0.0566	12.46	0.0547	7.35	0.0687
7.79	0.0550	13.47	0.0459	7.79	0.0694
8.30	0.0522	14.95	0.0363	8.30	0.0720
9.56	0.0475			8.96	0.0774
10.41	0.0440			9.56	0.0764
11.59	0.0411			10.01	0.0779
12.46	0.0390			10.41	0.0754
13.47	0.0364			11.29	0.0675
14.95	0.0331			11.59	0.0637
14.92	0.0324			12.46	0.0528
15.50	0.0339			13.47	0.0431
16.44	0.0315			14.95	0.0348
17.72	0.0325			14.92	0.0340
19.10	0.0319			14.92	0.0359
20.71	0.0283			15.50	0.0319
22.61	0.0289			15.50	0.0321
24.90	0.0265			16.44	0.0291
26.15	0.0255			16.44	0.0314
27.61	0.0243			17.72	0.0265
29.32	0.0242			19.10	0.0244

Table 5 Absorptivity of Chromium Sample (continued)

281 K		76.5 K		7.5 K	
Wavelength (μm)	Absorptivity	Wavelength (μm)	Absorptivity	Wavelength (μm)	Absorptivity
33.02	0.0228			20.71	0.0221
40.02	0.0224			22.61	0.0208
47.36	0.0179			24.90	0.0197
Absorptance After Cooldown				26.15	0.0164
				27.61	0.0151
9.56	0.0451			29.32	0.0138
13.77	0.0353			33.02	0.0133
				40.02	0.0098
				44.07	0.0032
				53.95	0.0022

it is calculated that, for example, for iron at 15 μm the error in relative reflectivity is 0.00015 which is an order of magnitude below the errors from other sources.

In calculating absorptivities from the measured relative reflectivities a further uncertainty is introduced in the value of the reflectivity of the gold reference mirror. From the values given in Table 1 it is seen that a further systematic error of 0.001 could thereby be introduced into the absorptivity. Total systematic error could therefore amount to ± 0.004 in the absorptivity.

6. Discussion of Experimental Results and Comparison with Theory

With the exception of chromium, the absorptivity data exhibit the characteristic wavelength and temperature dependence of transition metals; the same general trends have been observed at higher temperatures and may be summarized as: a temperature independent high absorptivity at short wavelengths decreasing monotonically toward longer wavelengths, where it becomes strongly temperature dependent. Where other data were available[13, 15, 31] these have also been plotted and it is seen that agreement varies from only fair for nickel to excellent for platinum at room temperature.

The unusual behavior of chromium at 76.5 K and 7.5 K deserves special comment. It appears that a resonance becomes effective at low temperatures. This point has already been discussed in the literature by Barker et al.[28] who measured the reflectivity from room temperature to 80 K. The dip in the reflectivity observed by these authors occurred at 10 μm in agreement with the present data. The data of figure 13 extend these measurements to lower temperatures and longer wavelengths and add accuracy to the measurement. The phonomenon has been attributed to the onset of antiferromagnetism below a critical temperature, the Néel temperature, which is about 312 K for chromium. The present data confirm the expectation of Barker at al. that the absorptivity should become independent of temperature below 80 K in the region of the absorptivity maximum. For present purposes it is apparent that the absorptivity of such a metal could not be predicted from the semiclassical theory of conduction electrons except perhaps at long wavelengths where the characteristic trend is again resumed. No calculations were therefore attempted for chromium.

For the remaining metals a comparison with theory was based upon the 2-band extension of the Anomalous Skin Effect theory. The equations were derived by one of us (M.C.J.) and Professor C.L. Tien at the University of California, Berkeley, and will be presented more fully in a future publication[29]. For the present we merely quote the final results.

In the Anomalous Skin Effect theory one calculates the complex surface impedance rather than the local complex conductivity customary in the classical case. In the classical limit the complex impedance for the 2-band case is given by

$$\underset{\sim}{Z}^{cl} = \frac{4\pi i\omega\tau_1 V_1}{W_1 c^2}\left[\eta + \frac{4}{3}(\xi_1 + \xi_{12})\right]^{-1/2} \qquad (1)$$

with the supplementary definitions

$$\xi_1 = \frac{i\alpha_1}{W_1^3}$$

$$\xi_{12} = \frac{\sigma_2 W_1}{\sigma_1 W_2}\,\xi_1$$

$$\alpha_1 = \frac{3\pi\omega\tau_1^2\sigma_1 V_1^2}{c^2}$$

$$\eta = \frac{-\epsilon_\infty \omega^2 \tau_1^2 V_1^2}{W_1^2 c^2}$$

$$W_1 = 1 + i\omega\tau_1$$

$$W_2 = 1 + i\omega\tau_2$$

Here ω is the circular frequency; c is the speed of light in vacuum; σ_1 is the classical static conductivity for the first electron band, V_1 its Fermi velocity and τ_1 its relaxation time. Similar quantities are subscripted 2 for the second band of electrons. ϵ_∞ is a phenomenologically introduced dielectric constant to take account of polarization of

core electrons and interband transitions. Equation (1) is completely equivalent to the theory of Roberts.

In the more general Anomalous Skin Effect theory assuming diffuse electron reflection at the boundary the complex impedance is given by the equation

$$\tilde{Z} = \frac{4\pi^2 i\omega\tau_1 V_1}{W_1 c^2} \left\{ \int_0^\infty \ell n \left[1 + \frac{\eta + \xi_1 \chi(t) + \xi_{12} \chi\left(\frac{W_1 t}{r W_2}\right)}{t^2} \right] dt \right\}^{-1} \quad (2)$$

where in addition to terms defined above for (1) we have $r = \tau_1 V_1 / \tau_2 V_2 \geq 1$ and $X(t) = \frac{1}{t^3} \left[-2t - i(1+t^2) \log \frac{1+it}{1-it} \right]$. From the complex impedance the absorptivity A for normal incidence is calculated from the equivalent form of the Fresnel formula

$$A = 1 - \left| \frac{Z_o - \tilde{Z}}{Z_o + \tilde{Z}} \right|^2 \quad (3)$$

where Z_o is the impedance of free space, $4\pi/c$.

In addition, the relaxation time was calculated from the equation given by Gurzhi[11] for the quantum mechanical interaction referred to on page 3 in view of the rather compelling evidence in its favor.[8,9] In the form used here we have

$$\tau = \left[\frac{1}{\tau_o} + \frac{1}{\tau^{cl}(\theta)} K(\omega, T) \right]^{-1} \quad (4)$$

where τ_o is the readily available d.c. value, $\tau^{cl}(\theta)$ is the classical value calculated at the Debye temperature θ, and $K(\omega, T)$ is the function

$$K(\omega, T) = 2\left(\frac{T}{\theta}\right)^5 \int_0^{\theta/T} V^4 \left(\frac{\frac{V}{\gamma} - 1}{e^{V-\gamma} - 1} - \frac{\frac{V}{\gamma} + 1}{e^{V-\gamma} + 1}\right) dV$$

with $\gamma = \hbar\omega/kT$. At low temperatures K varies from 0 at low frequencies to 2/5 for $\hbar\omega > k\theta$. Now, Roberts and Seban[15] found that ϵ_∞ and the empirical parameters representing the second conduction band had to be held constant with temperature in order to reproduce observed absorptivities. The scattering in this band therefore appears not to be due to phonon interaction so equation (4) was only applied to band-1. Equations (1) through (4) provide the theoretical framework for the calculations. They require the specification of certain material parameters. These are τ_1, σ_1, V_1, τ_2, σ_2, V_2. Now it was found in reference [29] that the parameters for band-2 could not be identified with known d-band parameters if anything close to the experimental absorptivity is to be calculated at short wavelength,and it was noted that, as far as this band is concerned, the theory is phenomenological; i.e., it is not known how these parameters could be estimated except from absorptivity data. Nevertheless the theory is useful if band-1 parameters may still be identified with the major charge carriers, the s-electrons, and if, following Roberts and Seban, band-2 parameters are taken to be independent of temperature. In this case the temperature dependence of

the absorptivity could still be predicted unambiguously from the d.c. conductivity and, furthermore, it is found that the long wavelength absorptivity is unaffected by the choice of these empirical parameters.

The following calculation scheme was therefore followed in a trial and error procedure by which best values for band-2 parameters were selected on the basis of the fit to the room temperature data.

For a given value of σ_2, σ_1 was calculated from the zero frequency constraint

$$\sigma_1 + \sigma_2 = \sigma_0 \tag{5}$$

where σ_0 is the d.c. conductivity for the pure annealed metal obtained from the literature.[30] On the assumption of a spherical Fermi surface τ_1 was calculated from the free electron formula

$$\sigma_1 = \frac{n_1 e^2 \tau_1}{m_1} \tag{6}$$

with the ratio n_1/m_1 obtained from the literature.[2] n_1 is the effective number of s-electrons and m_1 the effective mass. Finally V_1 was also obtained directly from the literature.[2] When the best fit had been obtained at room temperature the liquid helium temperature absorptivity required only the specification of the appropriate new value of σ_0 from the literature. Since the extensive literature on this property at liquid helium temperatures shows a wide variation, calculations were repeated for a value one third of the original value used. No significant change

was observed, showing that the theory is close to the temperature independent extreme anomalous limit. The values of the parameters used in the calculation are listed in Table 6. In place of relaxation times τ_1 and τ_2 equivalent wavelengths ($\lambda = 2\pi c\tau$) are given.

The results of the calculations are shown in figures 10, 11 and 12. In addition to the liquid helium temperature calculation described above, based on the 2-band Anomalous Skin Effect theory, the curve resulting from the classical limit, i.e., equation (1) is also shown and, for platinum (figure 12) we also show the corresponding curves with a frequency independent relaxation time to illustrate the contribution due to frequency dependence in equation (4).

Comparison with the data shows that for nickel and iron even at room temperature the calculation is only in qualitative agreement although the magnitude of the temperature shift is approximately correct. Furthermore, for these two metals the curves presented were calculated with n_1/m_1 decreased from the literature values. This had the effect of increasing the short wavelength absorptivity and decreasing the long wavelength absorptivity compared to the curves which were based on literature values of n_1/m_1. In fact, this quantity is not accurately known so that some latitude is permissable. Even so the room temperature fit is not good.

Table 6. Metal Parameters Used in Calculations

Parameter	Temperature	Nickel	Iron	Platinum
σ_0	295 K	1.278	0.918	0.864
(esu $\times 10^{17}$)	4 K	450	901	2.270
σ_2				
(esu $\times 10^{17}$)		0.10	0.07	0.07
λ_2				
(μm)		0.10	0.20	0.2
V_2				
(cm $sec^{-1} \times 10^8$)		0.0604	0.215	0.0715
$\sigma_1 = \sigma_0 - \sigma_2$	295 K	1.178	0.848	0.794
(esu $\times 10^{17}$)	4 K	450	901	2270
$\frac{n_1}{m_1}$				
($cm^{-3}\ g^{-1} \times 10^{50}$)		0.20	0.15	0.44
$\lambda_1 = \sigma_1 \frac{2\pi c m_1}{n_1 e^2}$	295 K	48	46.2	14.7
(μm)	4 K	18,400	49,100	42,200
V_1				
(cm $sec^{-1} \times 10^8$)		1.365	0.912	1.230
ϵ_∞		2.7	2.4	2.4

Note: Of these parameters σ_2, λ_2, and ϵ_∞ taken together are empirical; the rest are obtained from the literature or calculated as indicated.

In the case of platinum, without adjustment of n_1/m_1, the fit to the data at both room and liquid helium temperature is quite good over most of the wavelength range. At short wavelengths the data, particularly when taken together with those of Seban, are suggestive of some sort of resonance not taken into account by the theory and they diverge from the calculated curve at both temperatures.

For all three metals it is seen that at liquid helium temperatures the more general Anomalous Skin Effect theory is an improvement over the classical limit. It is noted also that the curves lie considerably higher, even at room temperature, when the frequency dependent relaxation time of equation (4) is used. The data therefore lend some further support to the quantum absorption mechanism and the fact that the infrared relaxation time cannot be directly related to the d. c. value. This is quite important for transition metals which mostly have high Debye temperatures and for which the quantum absorption would be more pronounced and to be expected even at room temperature.

7. Conclusions

1. Experimental data have been obtained for the normal spectral absorptivity of the transition metals nickel, iron, platinum and chromium at both room and liquid helium temperatures in the wavelength range 2. 5 to 50 μm. The absorptivity was derived from reflectivity measurements made relative to a room-temperature

vapor-deposited gold reference mirror. The absorptivity of the gold reference mirror was measured calorimetrically using infrared laser sources.

2. Various methods of surface preparation were investigated. The method selected for final data by the criterion of highest near infrared reflectivity was mechanical polishing with progressively finer grades of diamond abrasive followed by vacuum annealing at temperatures close to the published one hour recrystallization temperatures. In some cases repetition of the last stages of mechanical polishing and reannealing gave rise to even higher reflectivities.

3. The effect on the absorptivity of lowering the temperature was in all cases negligible at short wavelengths but a significant lowering at longer wavelengths. In the case of chromium an additional feature appears; an absorptivity maximum higher than the room temperature absorptivity occurs at about 10 μm. This feature, identified by others as due to the onset of antiferromagnetism, appears to be independent of temperature below liquid nitrogen temperature.

4. Calculations of the absorptivity based on a 2-band model were made. It was necessary to determine the material constants for the second band empirically. The first band was identified with

the s-electrons. The temperature and wavelength dependence of the absorptivities for nickel and iron could be represented only qualitatively for iron and nickel, but for platinum quite well if second band parameters were assumed to be temperature independent. The Anomalous Skin Effect theory was found to give a better account of the temperature dependence than the classical theory. In all cases it was necessary to calculate the relaxation time for s-electrons according to the theory of the quantum mechanical interaction due to Holstein and Gurzhi in order to achieve sufficiently high absorptivities.

8. References

1. P. F. Dickson and M. C. Jones, Infrared Spectral Reflectance of Metals at Low Temperatures, Cryogenics 8, 224-229 (1968).
2. N. F. Mott and H. Jones, The Theory of the Properties of Metals and Alloys, Clarendon Press, Oxford (1936) and Dover Publications Inc., New York, 110, (1958).
3. G. E. H. Reuter and E. H. Sondheimer, The Theory of the Anomalous Skin Effect in Metals, Proc. Roy. Soc. A195, 336-364 (1948).
4. R. B. Dingle, The Anomalous Skin Effect and the Reflectivity of Metals I., Physica 19, 311-347 (1953).
5. M. A. Biondi, Optical Properties of Copper and Silver at 4.2°K., Phys. Rev. 102, 964-967 (1956).
6. R. G. Chambers, The Anomalous Skin Effect, Proc. Roy. Soc. A215, 481 (1952).
7. H. E. Bennett, J. M. Bennett, E. J. Ashley and R. J. Motyka, Verification of the Anomalous-Skin-Effect Theory for Silver in the Infrared, Phys. Rev. 165, 755-764 (1968).
8. A. I. Golovashkin, Optical Properties of Lead at Low Temperatures, Soviet Physics, J. E. T. P., 21 (48), 548 (1965).
9. R. R. Joyce and P. L. Richards, Phonon Contribution to the Far-Infrared Absorptivity of Superconducting and Normal Lead, Phys. Rev. Letters 24, 1007 (1970).
10. T. Holstein, Optical and Infrared Volume Absorptivity of Metals, Phys. Rev. 96, 535 (1954).
11. R. N. Gurzhi, On the Theory of the Infrared Absorptivity of Metals, Soviet Physics, J. E. T. P., 6 (33), 506 (1958).
12. S. Roberts, Interpretation of the Optical Properties of Metal Surfaces, Phys. Rev. 100, 1667-1671 (1955).

13. S. Roberts, Optical Properties of Nickel and Tungsten and their Interpretation According to Drude's Formula, Phys. Rev. 114, 104-115 (1959).

14. A. H. Wilson, The Theory of Metals, Cambridge University, Press, London, 199 (1953).

15. R. A. Seban, The Emissivity of Transition Metals in the Infrared, J. Heat Transfer, Trans. ASME series C87, 173-176 (1965).

16. D. K. Edwards and N. Bayard de Volo, Useful Approximations for the Spectral and Total Emissivity of Smooth Bare Metals, Advances in Thermophysical Properties at Extreme Temperatures and Pressures, 174-188, ASME, New York (1965).

17. J. M. Bennett and E. J. Ashley, Infrared Reflectance and Emittance of Silver and Gold Evaporated in Ultrahigh Vacuum, Applied Optics 4, 221-224 (1965).

18. H. E. Bennett, Influence of Surface Roughness, Surface Damage, and Oxide Films on Emittance., Symposium on Thermal Radiation of Solids, NASA SP-55, Ed. S. Katzoff, 145-152, National Aeronautics and Space Administration, Washington, D. C., (1965).

19. M. C. Jones and D. C. Palmer, A Technique for the Measurement of Spectral Reflectances at Low Temperatures in the Infrared and Far Infrared, Progress in Astronautics and Aeronautics, Vol. 21, Ed. J. T. Bevans, 543-557, Academic Press (1969).

20. J. Talbot, The Annealing Behavior of High Purity Iron, Recovery and Recrystallization of Metals, L. Himmel (Ed.), 294, Gordon and Breach Science Publishers, Inc., New York (1963).

21. S. J. Rosenberg, Nickel and its Alloys, NBS Monograph 106, National Bureau of Standards, Washington, D. C., (1968).

22. E. Raub, Einfluss des Reinbeitsgrades von Platin auf Versfestigung, Erholung und Rekristallisation, Zeitschrift fur Metallkunde 55, 512 (1964).

23. D. J. Maykuth and A. Gilbert, Chromium and Chromium Alloys Report No. 234, Defense Metals Information Center, Battelle Memorial Institute, Columbus, Ohio (October 1, 1966) p 33.

24. A. L. Bloom, Gas Lasers, (J. Wiley, New York, 1968).

25. H. A. Gebbie, F. D. Findlay, N. W. B. Stone and J. A. Robb, Interferometric Observations on Far Infrared Stimulated Emission Sources, Nature 202, 169 (1964).

26. H. A. Gebbie, N. W. B. Stone and F. D. Findlay, A Stimulated Emission Source at 0.34 Millimetre Wave-length, Nature 202, 685 (1964).

27. V. G. Padalka and I. N. Shklyarevskii, Determination of the Microcharacteristics of Silver and Gold from the Infrared Optical Constants and the Conductivity at 82 and 295°K, Optics and Spectroscopy 11, 285 (1961).

28. A. S. Barker, B. I. Halperin and T. M. Rice, Antiferromagnetic Energy Gap in Chromium, Phys. Rev. Letters 20, 384 (1968).

29. M. C. Jones, Spectral Radiative Properties of Metals at Liquid Helium Temperatures, Ph. D. Thesis in preparation, University of California, Berkeley, California.

30. G. T. Meaden, Electrical Resistance of Metals. (Plenum Press, New York, 1965).

31. M. A. Biondi and A. I. Guobadia, Infrared Absorption of Aluminum, Copper, Lead and Nickel at 4.2°K, Phys. Rev. 166, 667-673 (1968).

PART II. LOW TEMPERATURE INFRARED REFLECTIVITY MEASUREMENTS FOR INDIUM ANTIMONIDE

1. Introduction

All III-V semiconducting compounds exhibit an infrared resonance frequency which is poorly understood except in a qualitative manner. The resonance is due to the interaction of the electric field of the light wave with the electric dipole moment of the crystal unit cell. This dipole moment will exist when the unit cell contains nonidentical atoms. The dipole moment in III-V semiconductors is thought to be associated with a polarized covalent bond but no calculations exist which predict the resonance or "reststrahlen" frequency of the oscillating dipoles. The purpose of the measurements reported here was an accurate determination of the reststrahlen frequency to be compared with a theoretical value calculated as described in Section 4. One of us (D. C. P.) has investigated this phenomenon of the "reststrahlen" frequency in indium antimonide experimentally at N. B. S. and theoretically with Dr. Neil Ashby at the University of Colorado. The theoretical crystal model proposed in Section 4 assumes that the crystal lattice sites are fixed except for the oscillation due to reststrahlen resonance. A correct model for high temperatures would include a shift in this resonance frequency due to interaction of the reststrahlen mode with thermal vibrations of the lattice. Experimental data for comparison with the theory

should therefore be taken at a low temperature.

2. Experimental

Using the low temperature reflectivity techniques described in Part I, the reflectance of indium antimonide vs. gold was measured at a temperature of 10.5 ± .3 K from 41 to 283 cm^{-1}. The reflectivity was measured to ± .5% and the wave number to ± .15 cm^{-1} in the spectral region crucial to the determination of the reststrahlen frequency (167 cm^{-1} - 283 cm^{-1}). The wave number resolution was held to 1.5 cm^{-1} over the region 180 cm^{-1} - 197 cm^{-1}. The indium antimonide sample was doped with tellurium and had a carrier concentration of 2.9×10^{16} cm^{-3} at 77 K.

The indium antimonide sample was approximately 1/8 inch thick and was mechanically polished with a series of abrasives, terminating with .3 micron alumina. The surface was finished by chemical polishing (2 gm. of iodine dissolved in 50 ml. methanol) for one minute to remove the material work-hardened by abrasion. The resulting mirror smooth surface deviated from perfect flatness by less than 1 micron over the 5/8 inch diameter central area struck by the light beam.

The wave number scale of the spectrophotometer was calibrated for each grating by recording the scale readings which correspond to multiple orders of the green line in the mercury spectrum. A computer program was written to provide the wave number $\bar{\nu} = F_g(d)$ for any

grating g and scale reading d. The function $F_g(d)$ was assumed to be a fifth order polynomial in d. The coefficients in F_g were evaluated by a least squares fit to the calibration data.

3. Data Analysis

The experimental reflectivity spectrum (See Fig. 1 and Table I) was compared to the reflectivity function derived from a classical Drude-Lorenz model:[1]

$$R(\Omega) = 100 \left| \frac{\epsilon^{1/2} - 1}{\epsilon^{1/2} + 1} \right|^2$$

where

$$\epsilon = \epsilon_1 + i\epsilon_2 , \quad \Omega = \bar{\nu}/\bar{\nu}_o$$

and

$$\epsilon_1 = \epsilon_\infty \left[1 + \frac{(\alpha - 1)(1 - \Omega^2)}{(1 - \Omega^2) + \Gamma_L^2 \Omega^2} - \frac{\Omega_p^2}{\Omega^2 + \Gamma_E^2} \right]$$

$$\epsilon_2 = \epsilon_\infty \left[\frac{\Gamma_L \Omega (\alpha - 1)}{(1 - \Omega^2)^2 + \Gamma_L^2 \Omega^2} + \frac{\Gamma_E \Omega_p^2}{\Omega^3 + \Gamma_E^2 \Omega} \right]$$

$\bar{\nu}$ = frequency in cm^{-1} (wave numbers)
$\bar{\nu}_o$ = reststrahlen frequency
ϵ = complex dielectric constant
ϵ_1 = real part of the dielectric constant
ϵ_2 = imaginary part of the dielectric constant
ϵ_∞ = dielectric constant when $\bar{\nu} \gg \bar{\nu}_o$ but less than interband transition frequencies

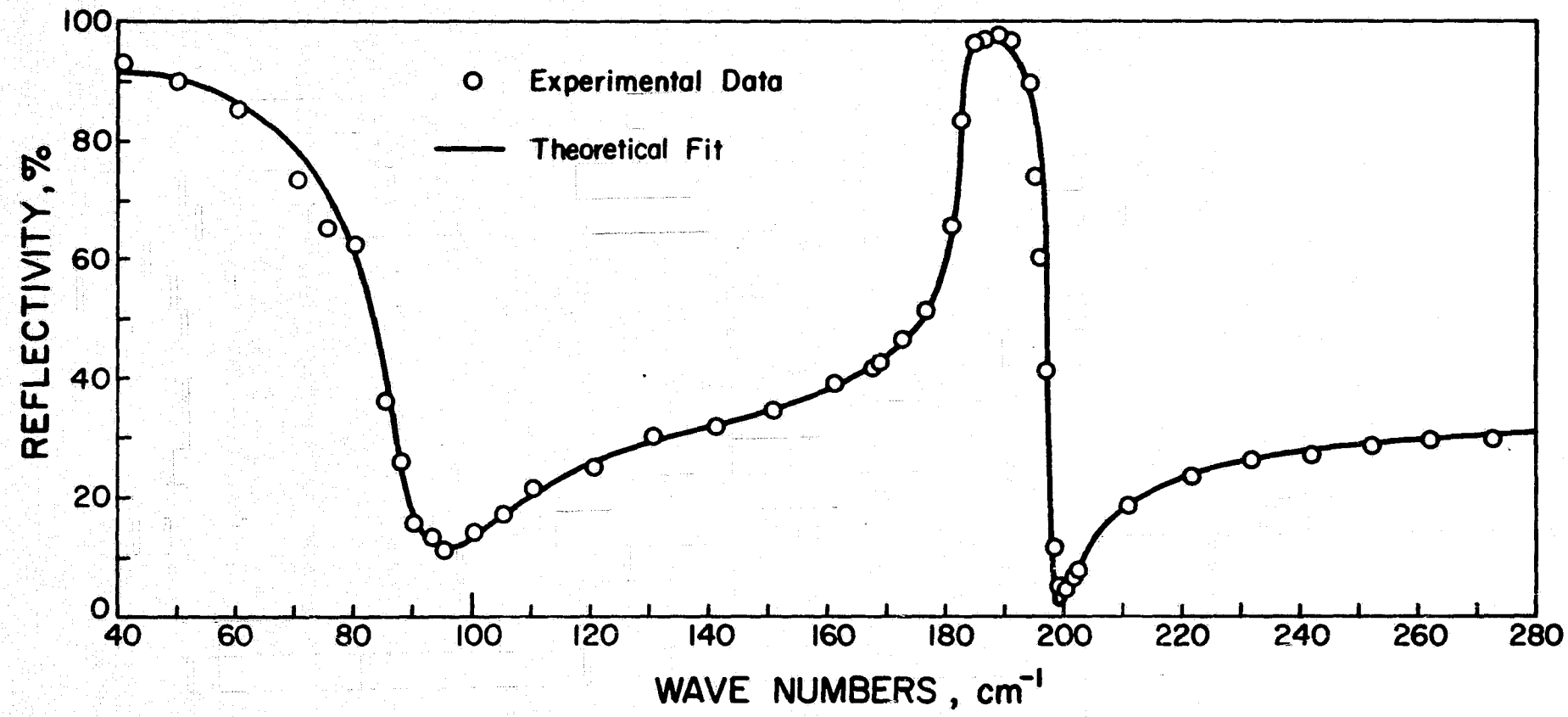

Figure 1. Experimental Reflectivity of Indium Antimonide Sample at 10.5 K and Theoretical Fit

Table 1. Reflectivity of Indium Antimonide at 10.5 K

Wavenumber (cm^{-1})	Resolution (cm^{-1})	Measured Reflectivity (%)	Calculated Reflectivity (%)
41.2	1	93.0	91.13
50.3	1	90.2	89.30
60.4	1	85.4	85.71
70.5	1	73.3	78.12
75.7	1	65.3	70.60
80.2	1	62.7	59.56
85.1	1	36.1	39.46
88.1	1	26.0	25.14
90.1	1	15.6	17.32
93.3	1	13.2	11.74
95.1	1	11.2	11.27
100.3	2	14.1	13.82
105.3	2	17.2	17.26
110.3	2	21.3	20.33
120.6	2	25.2	25.22
130.6	2	30.1	28.83
140.9	3	31.9	31.94
150.9	4	34.6	34.95
161.1	4	39.1	38.74
167.3	4	41.8	42.05
168.8	3	42.8	43.10
172.5	3	46.4	46.39
176.6	3	51.6	52.33
180.8	1.5	65.5	65.38
182.6	1.5	83.5	81.89
184.9	1.5	96.5	96.90
186.7	1.5	97.0	97.08
189.0	1.5	98.0	96.43
190.9	1.5	96.9	95.16
194.1	1.5	89.7	88.56

Table 1. (continued)

Wavenumber (cm^{-1})	Resolution (cm^{-1})	Measured Reflectivity (%)	Calculated Reflectivity (%)
195.0	1.5	73.9	83.50
195.9	1.5	60.1	73.73
196.9	1.5	41.1	51.07
198.2	2.0	11.8	2.63
199.2	2.0	4.9	1.15
200.1	2.0	4.3	3.07
201.5	2.0	6.2	6.38
202.4	2.0	7.7	8.33
210.7	2.0	18.3	18.36
221.4	2.0	23.4	23.50
231.6	3.0	26.1	26.05
241.9	3.0	27.0	27.66
252.2	3.0	28.5	28.79
262.0	3.0	29.5	29.60
272.8	3.0	29.8	30.28
283.0	3.0	30.4	30.81

ϵ_o = lattice dielectric constant when $\bar{\nu} \ll \bar{\nu}_o$

$\bar{\nu}_p$ = carrier electron plasma frequency

$\alpha = \epsilon_o/\epsilon_\infty$

$\Omega_p = \bar{\nu}_p/\bar{\nu}_o$

Γ_ϵ = carrier electron damping constant

Γ_L = lattice damping constant

The reflectivity function $R(\Omega)$ contains six empirical parameters which were determined by a least squares fit to the reflectivity data. The values of these parameters are the major results of this experiment.

$$\Gamma_L = 0.00254$$
$$\alpha = 1.13$$
$$\Gamma_\epsilon = 0.070 \pm 0.005$$
$$\Omega_p = 0.528 \pm 0.005$$
$$\epsilon_\infty = 15.4 \pm 0.9$$
$$\bar{\nu}_o = 183.0 \pm 0.2 \text{ cm}^{-1}$$

The limits placed on the last four parameters are 95% confidence intervals established by analyzing the scatter of the experimental reflectivity data. The variances σ^2 of the parameters were determined from experimental scatter by a second least squares fit. Reliable values for σ_{Γ_L} and σ_α were not obtainable by this technique. We conclude that the $R(\Omega)$ fit is not sensitive to Γ_L and α, and their quoted values are of undetermined accuracy. The reststrahlen frequency $\bar{\nu}_o$ is of central interest and can claim greater accuracy than the previous result $\bar{\nu}_o = 184.7 \pm 3 \text{ cm}^{-1}$ of Hass and Henvis [2].

4. Theory of the Reststrahlen Frequency

An approximate quantum mechanical model for the InSb crystal has been developed[3] and incorporated into a computer program to calculate the crystal binding energy. The approach is similar to that of Coulson, Redei and Stocker[4] in their calculation of the binding energy of boron nitride. Each covalent bond of the crystal is represented by a molecular orbital composed of adjacent SP^3 hybrid atomic orbitals. The wave function Ψ of the entire crystal is assumed to be an antisymmetrized product of these bond wave functions. The binding energy of the crystal is then the expectation value of the crystal Hamiltoman:

$$E = \langle \Psi \mid H \mid \Psi \rangle \ .$$

This basic scheme proposed by CRS has been modified to apply to crystals composed of heavier atoms where there are many electrons which do not participate in the bonds. The valence electrons are required to remain outside a spherically symmetric core containing 46 electrons for indium or antimony. The ratio of the core radii for indium and antimony is determined by examination of the Hartree-Fock-Slater atomic wave functions[5]. The core radii are then fixed by requiring that the crystal binding energy have a minimum at the experimentally determined nearest neighbor distance 2.81 Å.

Calculations are currently under way to determine the proper core radii. The bond wave function contains five independent parameters which are varied to minimize E. The variational principle assures us that the lowest value of E corresponds to the best wave function of the form assumed. Our model is sufficiently simpler than that of CRS to make such variation feasible in terms of the computer time required.

Once the core sizes are found, this model should allow approximate calculations of the valence electron density in the crystal, its compressibility and the reststrahlen frequency. For example: To calculate $\overline{\nu}_o$ one must examine the shape of the binding energy curve as the indium and antimony atoms in a unit cell oscillate under the influence of an electromagnetic wave. The second derivative of E with respect to the distance between indium and antimony cores determines the value of $\overline{\nu}_o$. Although the model proposed is crude, this is a more fundamental approach to the calculation of $\overline{\nu}_o$ than has previously been attempted.

The theoretical and experimental work described in this report will be documented in the author's thesis at the University of Colorado.

5. References

1. Born and Huang, Dynamical Theory of Crystal Lattices, Oxford (1954).
2. Hass, M. and Henvis, B. W., J. Phys. Chem. Solids 23, 1099, (1962).
3. Ashby, N., Bohlanger, P., Biagi, P., Bartel, L., and Palmer, D. C., Theoretical Study of the Radiative Emissivity of Materials. Final Report to the National Aeronautics and Space Administration, Contract No. NAS8-20365 (1970).
4. Coulson, C. A., Redei, L. B. and Stocker, D., Proceedings of The Royal Society, A270, 357 (1962).
5. Herman, F. and Skillman, S., Atomic Structure Calculations, Prentice-Hall, (1963).

ACKNOWLEDGEMENT

We are pleased to acknowledge the assistance of Mr. Fred W. Windmoeller and of Mr. Earl R. Ballinger in the experimental work.